Source characteristics of the 6 June 2000 Orta–Çankırı (central Turkey) earthquake: a synthesis of seismological, geological and geodetic (InSAR) observations, and internal deformation of the Anatolian plate

T. TAYMAZ[1], T. J. WRIGHT[2], S. YOLSAL[1], O. TAN[3], E. FIELDING[4] & G. SEYİTOĞLU[5]

[1]*Department of Geophysics, İstanbul Technical University, Maslak-TR 34469, İstanbul, Turkey (e-mail: taymaz@itu.edu.tr)*

[2]*Department of Earth Sciences, University of Oxford, Parks Road, Oxford OX1 3PR, UK*

[3]*TÜBİTAK-Marmara Research Centre, 41470 Gebze, Kocaeli, Turkey*

[4]*Jet Propulsion Laboratory, 4800 Oak Grove Drive, Caltech, Pasadena, CA 91109, USA*

[5]*Department of Geological Engineering, Ankara University, 06100 Ankara, Turkey*

Abstract: This paper is concerned with the seismotectonics of the North Anatolian Fault in the vicinity of the Orta–Çankırı region, and consists of a study of a moderate-sized (Mw = 6. 0) earthquake that occurred on 6 June 2000. The instrumental epicentre of this earthquake is far from the North Anatolian Fault Zone (NAFZ), and rapid focal mechanism solutions of USGS–NEIC and Harvard-CMT also demonstrate that this earthquake is not directly related to the right-lateral movement of the North Anatolian Fault. This earthquake is the only instrumentally recorded event of magnitude (Mw) >5.5 since 1900 between Ankara and Çankırı, and therefore provides valuable data to improve our understanding of the neotectonic framework of NW central Anatolia. Field observations carried out in the vicinity of Orta town and neighbouring villages immediately after the earthquake indicated no apparent surface rupture, but the reported damage was most intense in the villages to the SW of Orta. We used teleseismic long-period P- and SH-body waveforms and first-motion polarities of P-waves, broadband P-waves, and InSAR data to determine the source parameters of the 6 June 2000 (Orta–Çankırı, t_o = 02:41:53.2, Mw = 6. 0) earthquake. We compared the shapes and amplitudes of long-period P- and SH-waveforms recorded by GDSN stations in the distance range 30–90°, for which signal amplitudes were large enough, with synthetic waveforms. The best-fitting fault-plane solution of the Orta–Çankırı earthquake shows normal faulting with a left-lateral component with no apparent surface rupture in the vicinity of the epicentre. The source parameters and uncertainties of this earthquake were: Nodal Plane 1: strike 2° ± 5°, dip 46° ± 5°, rake –29° ± 5°; Nodal Plane 2: strike 113°, dip 70°, rake –132°; principal axes: P = 338° (48°), T = 232° (14°), B = 131° (39°); focal depth 8 ± 2 km (though this does not include uncertainty related to velocity structure), and seismic moment $M_o = (140–185) \times 10^{16}$ N m. Furthermore, analysis of a coseismic interferogram also allows the source mechanism and location of the earthquake to be determined. The InSAR data suggest that the north–south fault plane (Nodal Plane 1 above) was the one that ruptured during the earthquake. The InSAR mechanism is in good agreement with the minimum misfit solution of P- and SH-waveforms. Although the magnitude of slip was poorly constrained, trade-off with the depth range of faulting accurred such that solutions with a large depth range had small values of slip and vice versa. The misfit was small and the geodetic moment constant for fault slips greater than *c*. 1 m. The 6 June 2000 Orta–Çankırı earthquake occurred close to a restraining bend in the east–west-striking rightlateral strike-slip fault that moved in the much larger earthquake of 13 August 1951 (Ms = 6.7). The faulting in this anomalous earthquake could be related to the local geometry of the main strike-slip system, and may not be a reliable guide to the regional strain field in NW central Turkey. We tentatively suggest that one possible explanation for the occurrence of the 6 June 2000 Orta–Çankırı earthquake could be localized clockwise rotations as a result of shear of the lower crust and lithosphere.

The epicentre of the 6 June 2000 Orta earthquake (Mw = 6.0) is far from the North Anatolian Fault Zone (Figs 1 and 2). Rapid focal mechanism solutions of USGS–NEIC and Harvard-CMT also demonstrate that this earthquake is not directly related to the right-lateral movement of the North Anatolian Fault (Fig. 2; Taymaz *et al.* 2002*a*, *b*). Field observations carried out in Orta town and

From: TAYMAZ, T., YILMAZ, Y. & DILEK, Y. (eds) *The Geodynamics of the Aegean and Anatolia.* Geological Society, London, Special Publications, **291**, 259–290.
DOI: 10.1144/SP291.12 0305-8719/07/$15.00

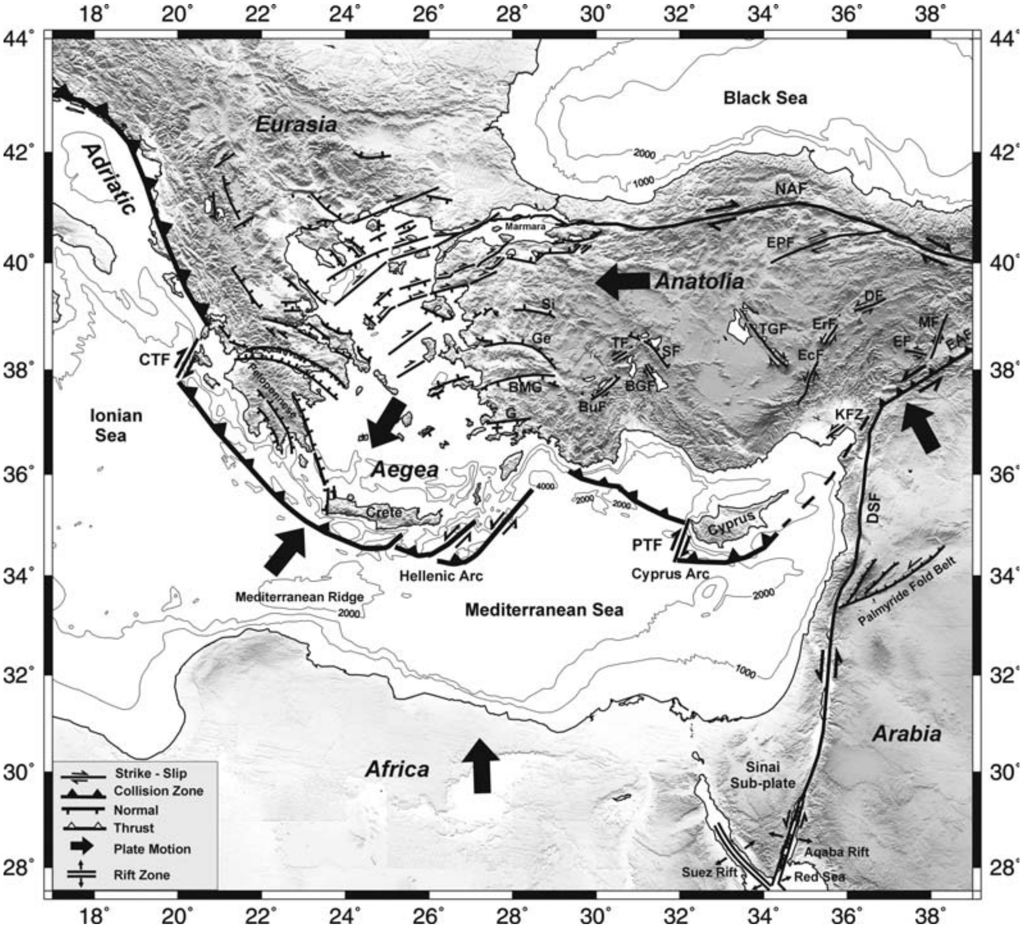

Fig. 1. Summary sketch map of the faulting and bathymetry in the Eastern Mediterranean region, compiled from our observations and those of Le Pichon *et al.* (1984, 2001), Şengör *et al.* (1985), Mercier *et al.* (1989), Taymaz *et al.* (1990, 1991*a*, *b*, 2002*a*, *b*), Şaroğlu *et al.* (1992), Taymaz & Price (1992), Jackson (1994), Price & Scott (1994), Alsdorf *et al*. (1995), Papazachos *et al.* (1998), Kurt *et al.* (1999, 2000), McClusky *et al.* (2000), Taymaz & Tan (2001), and Demirbağ *et al.* (2003). NAF, North Anatolian Fault; EAF, East Anatolian Fault; DSF, Dead Sea Fault; EPF, Ezinepazarı Fault; PTF, Paphos Transform Fault; CTF, Cephalonia Transform Fault; G, Gökova Fault; BMG, Büyük Menderes Graben; Ge, Gediz Graben; Si, Simav Graben; BuF, Burdur Fault; BGF, Beysehir Gölü Fault; TF, Tatarlı Fault; SF, Sultandağ Fault; TGF, Tuz Gölü Fault; EcF, Ecemiş Fault; ErF, Erciyes Fault; DF, Deliler Fault; EF, Elbistan Fault; MF, Malatya Fault; KFZ, Karataş–Osmaniye Fault Zone.

the neighbouring villages immediately after the earthquake indicated no apparent surface rupture, but the damage was most intense in the villages to the SW of Orta. To explain the cause of this earthquake the regional neotectonic framework should be taken into account. There are three main neotectonic elements in NW central Anatolia that correspond to the regional earthquake epicentre distribution ($M > 2$) between 1964 and 2000 (Fig. 2). The first is the well-known North Anatolian Fault Zone (NAFZ), which has the ability to generate earthquakes with magnitudes >5. The second main tectonic element is the Kırıkkale–Erbaa Fault Zone (KEFZ), which is responsible for the 10 June 1985, 14 February 1992 and 14 August 1996 earthquakes. The third tectonic element is a NNE–SSW-trending pinched crustal wedge between Ankara and Çankırı (see below). Its neotectonic importance was not accurately recognized until recently (Seyitoğlu *et al.* 2000, 2001). The closer distribution of epicentre locations (Fig. 2) along the line of Ankara and Çankırı corresponds to the NNE–SSW-trending İzmir–Ankara suture zone.

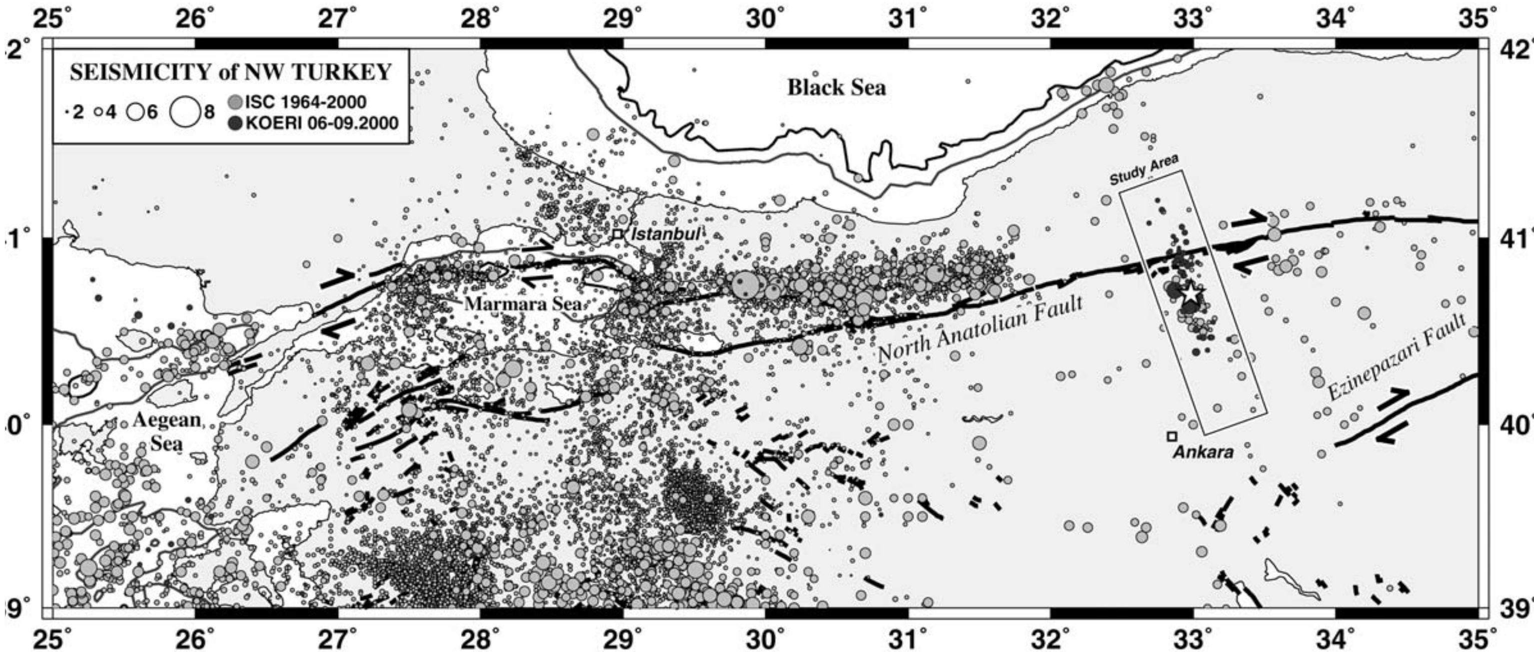

Fig. 2. Seismicity of NW Turkey and the character of the North Anatolian Fault (NAF; after Şaroğlu *et al.* 1992) reported by ISC during 1964–2000 for M >2 superimposed on a shaded relief map derived from the GTOPO-30 Global Topography Data from USGS. Bathymetry data are from Smith & Sandwell (1997). Geographical location of the study area is outlined by a rectangular box. The anomalous seismic activity (Kandilli Observatory) orthogonal to the trace of the NAF should be noted. Star indicates the instrumental epicentre of 6 June 2000 Orta–Çankırı earthquake reported by the USGS.

The 6 June 2000 Orta earthquake is the only instrumentally recorded event that has magnitude >5 since 1900 between Ankara and Çankırı, and therefore provides valuable data on the neotectonic framework of NW central Anatolia. In this paper, we first introduce the overall regional tectonic framework and then present seismological and InSAR investigations of the 6 June 2000 Orta–Çankırı earthquake. Finally, its implications on the internal deformation of the Anatolian plate will be discussed.

Neotectonic framework of NW central Anatolia

This section generally focuses on the less well-known reactivated section of the Izmir–Ankara suture zone between Ankara and Çankırı rather than relatively well-known structures such as the North Anatolia Fault (Ambraseys 1970; Ambraseys & Jackson 1998; McKenzie 1969, 1970; Nowroozi 1972; Şengör 1979; Stein *et al.* 1997; Taymaz *et al.* 2002*a*, *b*, 2004) and its splay, the Kırıkkale–Erbaa Fault (Figs 3 and 4; Polat 1988).

The remnant of the Neo-Tethyan ocean known as the Izmir–Ankara–Erzincan suture trends approximately east–west to the west of Ankara. Further to the east, it turns nearly 90° and has a NNE trend towards Çankırı (Figs 3 and 4). Although synorogenic basin development related to the closure of the northern branch of the Neo-Tethyan ocean during Cretaceous to Eocene time has been discussed (Şengör & Yılmaz 1981), there are few studies on the detailed post-collisional evolution of NW central Turkey. Okay & Tüysüz (1999) have recently studied this suture of northern Turkey and reported that the Tethyan subduction–accretion complexes along the İzmir–Ankara–Erzincan suture around Çankırı form a 5–10 km wide tectonic belt, which circles and radially thrusts the Eocene–Miocene sedimentary rocks of the Çankırı Basin, resulting in a large loop of the suture (Fig. 3). Furthermore, the Senonian andesitic volcanism observed in the northern parts of the Sakarya zone is thought to be related to northward subduction of the along İzmir–Ankara–Erzincan ocean. Palaeomagnetic data within the Sakarya Zone also indicate that it was close to the Laurasian margin during Liassic and Late Cretaceous time (Sarıbudak, 1989; Channel *et al.* 1996; Erdoğan *et al.* 1996). Although there is a considerable number of studies on the synorogenic basin development related to the closure of the northern branch of the Neo-Tethyan ocean during Cretaceous to Eocene time (e. g. see Görür *et al.* 1998, for a summary) there is only a limited number of field-oriented studies on the post-collisional evolution of NW central Turkey.

Koçyiğit (1991*a*, *b*, 1992) and Koçyiğit *et al.* (1995) proposed that intracontinental convergence related to the closure of the Neo-Tethyan ocean continued until the Late Pliocene, and called this the 'Ankara Orogenic Phase'. This suggestion was based on the south-vergent thrusting of the east–west-trending Izmir–Ankara suture zone over Neogene sedimentary units towards the east and west in the western margin of the Çankırı basin. Koçyiğit *et al.* (1995) also claimed that the sedimentary units were deposited in thrust-related basins. After the Late Pliocene, intracontinental convergence gave way to an extensional regime as indicated by the NE–SW-trending normal faults with related horizontal Pliocene deposits SW Çankırı (Koçyiğit *et al.* 1995).

However, Seyitoğlu *et al.* (1997) demonstrated that south-vergent thrusting of the suture zone does not exist NW of Ankara and argued that intercontinental convergence must have been ceased before Miocene times because Miocene to Pliocene geochemical evolution of the Galatia volcanic series (Wilson *et al.* 1997; Gürsoy *et al.* 1999) shows lithospheric thinning rather than thickening in the region. Alternatively, an extensional regime as a result of orogenic collapse has been proposed during Early Miocene–Pliocene time with emphasis on a post-Pliocene NAFZ effect on the region (Seyitoğlu *et al.* 1997). In addition, recent work (Seyitoğlu *et al.* 2000) has shown that the NNE–SSW-trending section of the İzmir–Ankara suture zone between Ankara and Çankırı has been reactivated as a east-vergent tectonic sliver that fragments and deforms Miocene–early Pliocene basin deposits. Thrust-related younger clastic deposits unconformably overlie the older deformed sediments in front of the tectonic sliver SE of Çankırı (Fig. 4c; Polat 1988). This latest east-vergent thrusting of the NNE–SSW-trending sector of the Izmir–Ankara suture is related to the NW–SE contraction caused by the movements of the right-lateral North Anatolian Fault and its splay, the Kırıkkale–Erbaa Fault Zone (Fig. 4c). Between these two strike-slip fault zones internal deformation of the Anatolian plate was mostly taken up by the weaker zones of the Neo-Tethyan orogeny.

The overall neotectonic framework of north central Anatolia is controlled mainly by splay faults of the NAFZ. The splay faults from SE to NW are the Almus Fault Zone (Bozkurt & Koçyiğit 1996), Ezinepazarı–Sungurlu Fault Zone, Kızılırmak Fault Zone and Laçin Fault Zone. They bifurcate from the NAF, and divide the Anatolian Block into east–west-trending wedge-like blocks that are deforming internally and rotating in a counter-clockwise sense (Tatar *et al.* 1995; Bozkurt & Koçyiğit 1996; Piper *et al.* 1996; Kaymakçı 2000). Chorowicz *et al.* (1999)

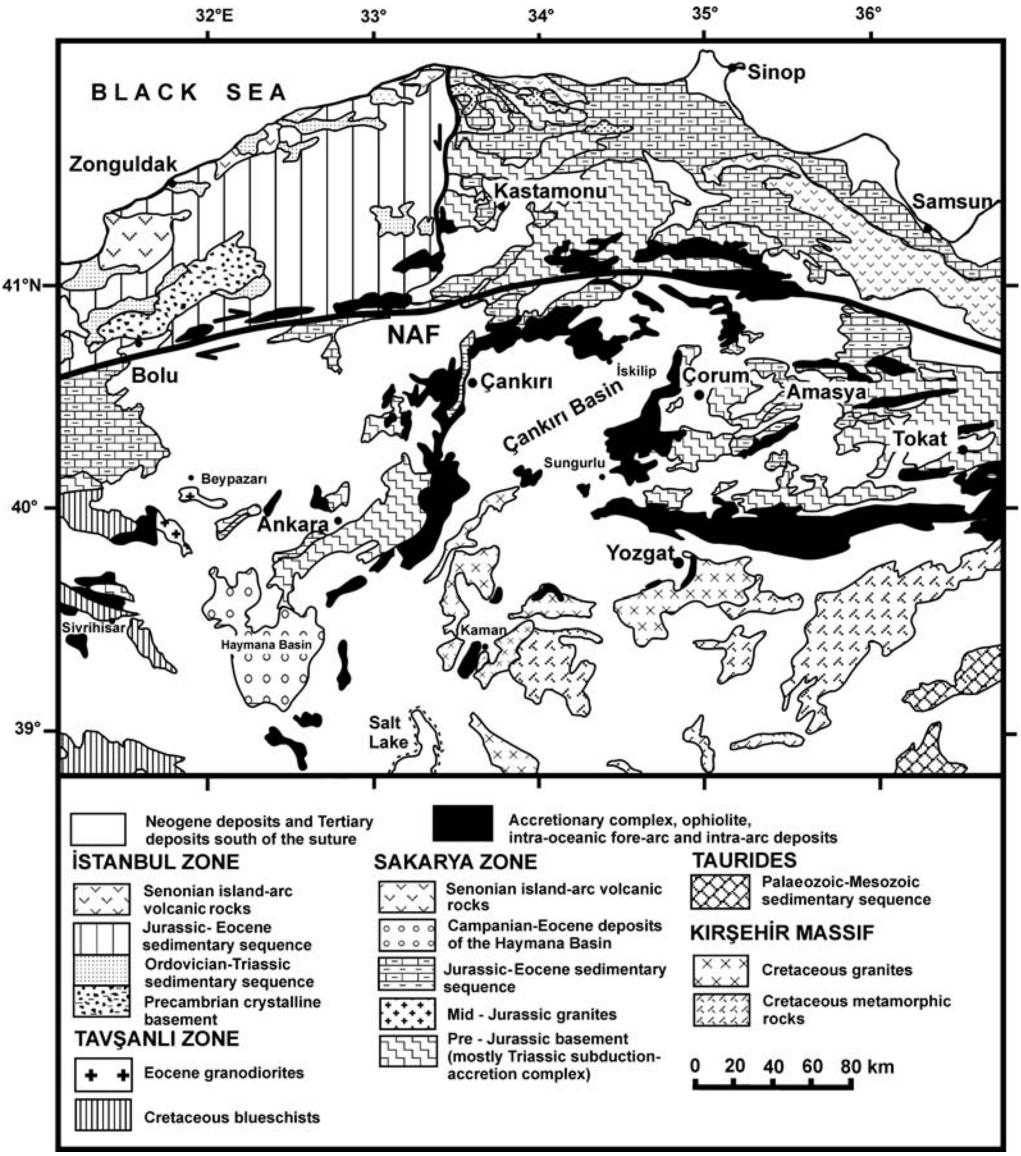

Fig. 3. Summary geological map of Çankırı Basin, central Turkey, and surrounding regions (reproduced with permission from Okay & Tüysüz (1999)).

interpreted these splays in a different way, as an element of extensional escape wedges, and suggested that the Anatolian Block is pulled by the Hellenic trench rather than pushing from the east because of collision of the Arabian and Eurasian plates.

Apart from these splays, nearly north–south-trending tectonic lines play an important role in the neotectonic framework of the region. However, there are varying descriptions and interpretations of these lines. These wedges are dissected by north–south-trending faults, which further complicate the deformation styles of the Anatolian Block in this region. The most important of these faults are the Eldivan Fault Zone (Kaymakçı 2000; Kaymakçı *et al.* 2003) and the Dodurga Fault Zone (Koçyiğit *et al.* 2001).

Seyitoğlu *et al.* (2000, 2001) described a NNE–SSW-trending east-vergent pinched crustal wedge between Ankara and Çankırı. The western margin

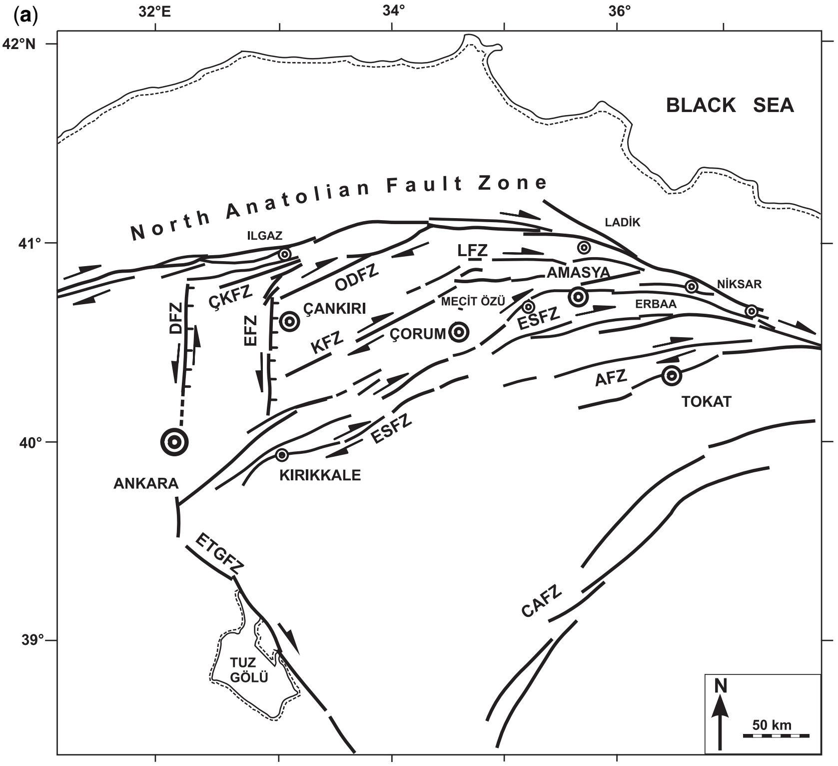

Fig. 4. (**a**) Map showing major structural elements of central Anatolia. Bold lines are strike-slip faults with arrows showing relative motion (after Bozkurt 2001). (**b**) Summary tectonic map of NW central Anatolia compiled from our observations and those of Şaroğlu *et al.* (1992), Gökten *et al.* (1996), Emre *et al.* (2000), and Koçyiğit *et al.* (2001). Main faults are marked with continuous lines. (**c**) Simplified main neotectonic elements of NW central Anatolia, North Anatolian Fault Zone (NAFZ), Kırıkkale–Erbaa Fault Zone (KEFZ), and the cause of the east-vergent tectonic sliver between Ankara and Çankırı. NW–SE-trending greatest principal stress (σ_1) is created by the NAFZ and KEFZ and activates the east-vergent tectonic sliver. 1, Neo-Tethyan suture zone; 2, Galatia volcanic complex (after Seyitoğlu *et al.* 2000).

of this wedge is limited by west-dipping normal faults but its eastern margin is a thrust that controls the accumulation of Late Pliocene–Pleistocene clastic deposits that unconformably overlie deformed Neogene successions in the western Çankırı basin (Fig. 3; Sen *et al*. 1998; Nemec & Kazancı 1999). Seyitoğlu *et al.* proposed that the thrusting and the related deformations in this region are linked with the post-Late Pliocene neotectonic pinched crustal wedge rather than intracontinental convergence (i.e. the Ankara orogenic phase). This wedge is developed as a result of the NW–SE contraction caused by the movements of the right-lateral NAFZ and its splay, the Kırıkkale–Erbaa Fault Zone (Fig. 4c).

In the same area, Kaymakçı (2000) re-mapped double-vergent thrusting towards the east and west after Akyürek *et al.* (1980). These inverted structures were interpreted as a consequence of the NNE–SSW-trending sinistral strike-slip Eldivan Fault Zone and they suggest that this fault zone was created by a major principal stress (σ_1) oriented NW–SE owing to transcurrent tectonics (Fig. 4c). Adıyaman *et al.* (2001) named the same fault zone the Korgun Fault, and considered that it plays an important role in creating the extensional escape wedges that moved to the SW during Early–Middle Miocene times and to WSW during Late Pliocene–Plio-Quaternary times (Fig. 4). West of the Eldivan or Korgun Fault, the north–south-trending Dodurga Fault has been mapped and nominated as a cause of the Orta earthquake (Fig. 4, Emre *et al.* 2000; Koçyiğit *et al.* 2001). The Dodurga Fault Zone (DFZ) bifurcates from the Çerkeş–Kurşunlu segment of the NAFZ around Çerkeş.

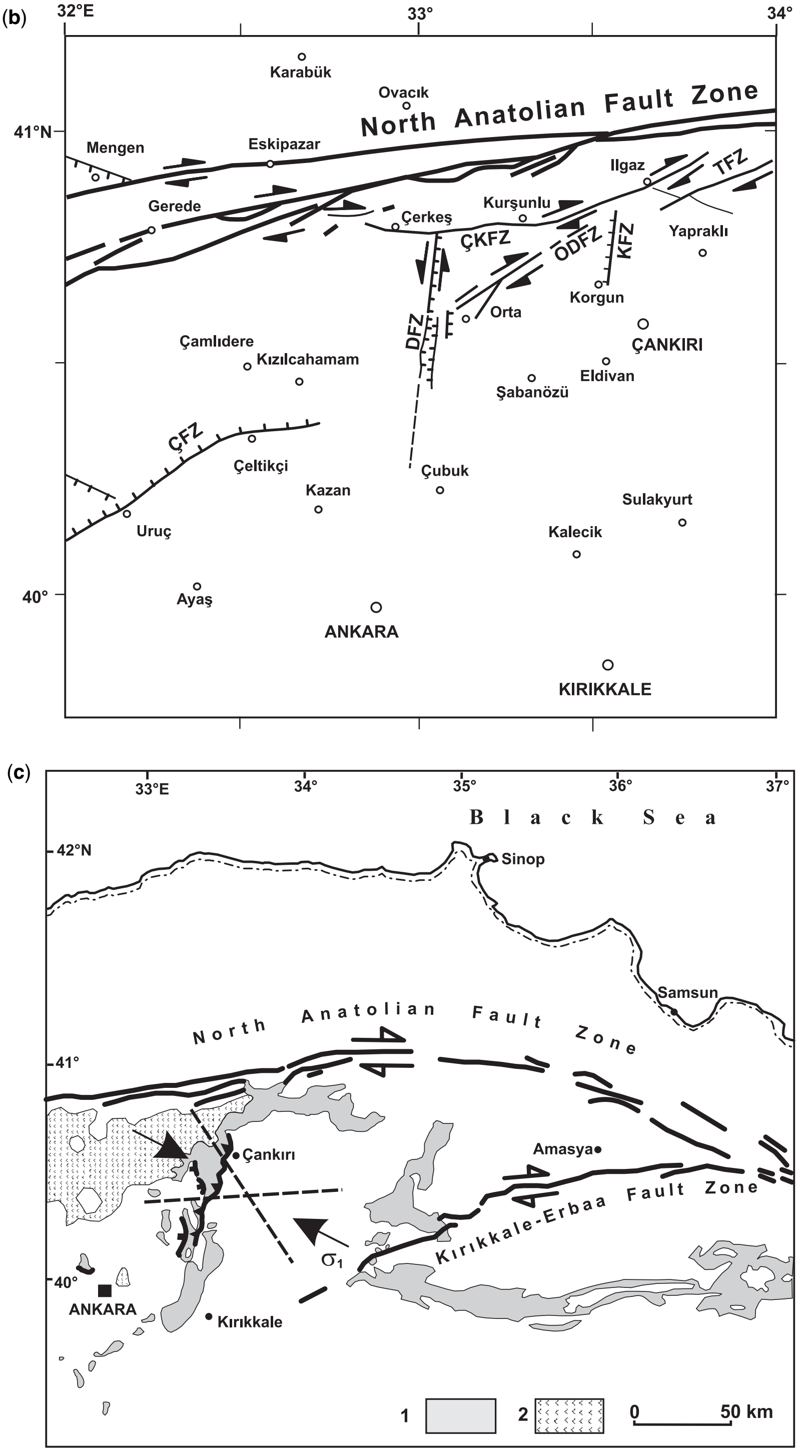

Fig. 4. *Continued.*

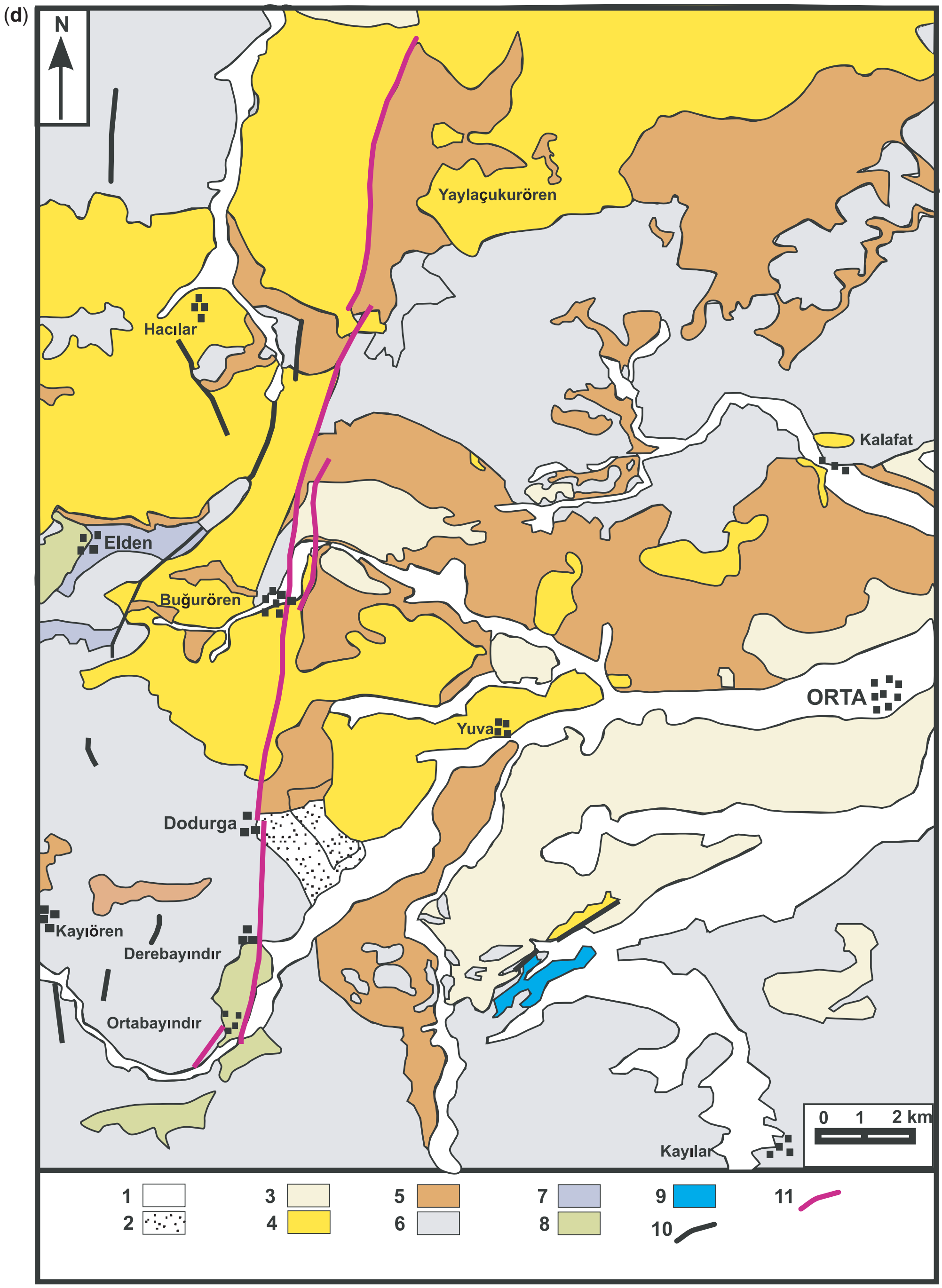

Fig. 4. *Continued.* (**d**) Simplified geological map of western part of Orta (Çankırı) and surrounding regions (modified after Türkecan *et al.* 1991; Emre *et al.* 2000): 1, alluvium (Quaternary); 2, alluvial fan (Quaternary); 3, conglomerate, sandstone, mudstone and limestone (Pliocene); 4, basalt (Pliocene); 5, conglomerate, sandstone, mudstone, limestone, and evaporite (Miocene); 6, andesite, basalt, rhyolite, dacite and pyroclastic deposits (Miocene); 7, andesite, basalt, dacite and pyroclastic deposits (Eocene); 8, sandstone, mudstone, limestone olistostrome (Late Cretaceous); 9, metadetrital deposits (Triassic), 10, faults; 11, Dodurga Fault.

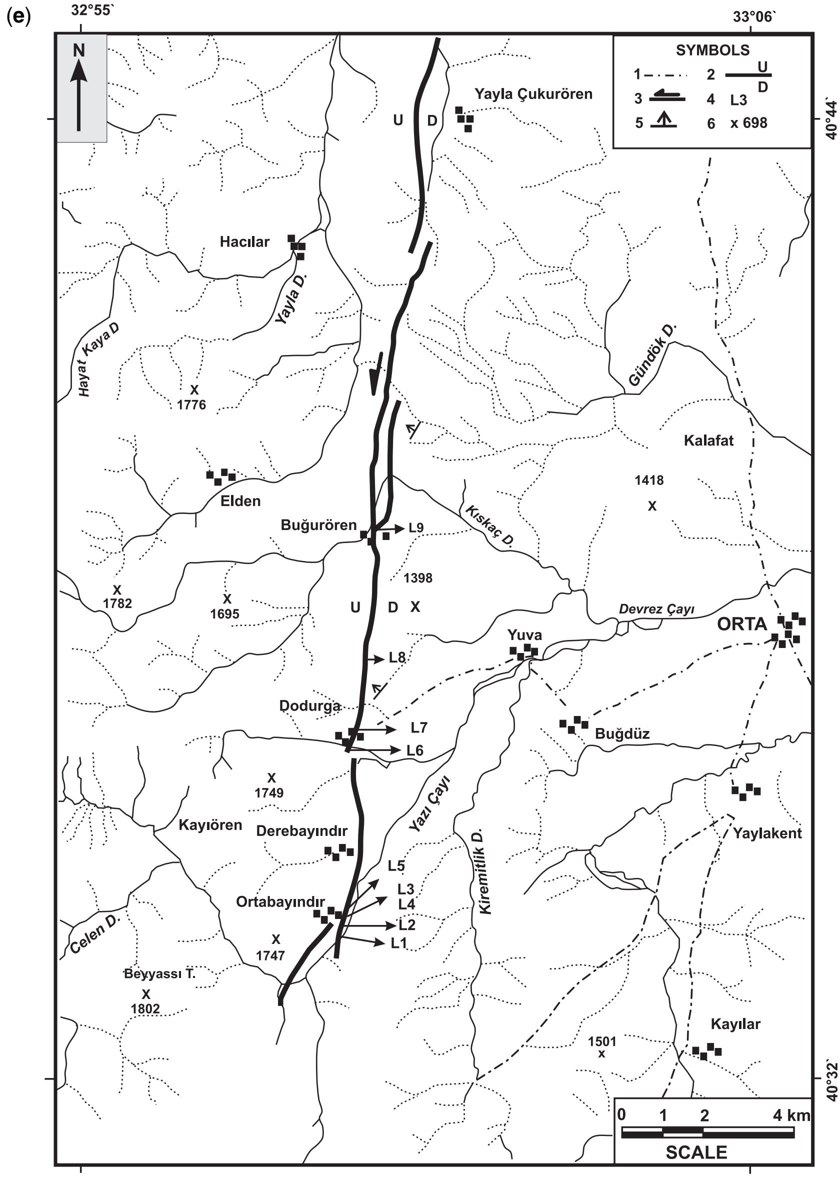

Fig. 4. *Continued.* (**e**) Detailed map of the Dodurga Fault (after Emre *et al.* 2000): 1, road; 2, up side (U) or down side (D); 3, left-lateral offset; 4, localities of observation sites; 5, direction of tilt; 6, elevation marks. AFZ, Almus Fault Zone; ÇFZ, Çeltikçi Fault Zone; ÇKFZ, Çerkeş–Kurşunlu Fault Zone; DFZ, Dodurga Fault Zone; EFZ, Eldivan Fault Zone; ESFZ, Ezinepazarı–Sungurlu Fault Zone; ETGFZ, Ezinepazarı–Tuz Gölü Fault Zone; ODFZ, Orta–Devrez Fault Zone; KFZ, Korgun Fault Zone; LFZ, Laçin Fault Zone; TFZ, Tosya Fault Zone; CAFZ, Central Anatolian Fault Zone.

The DFZ is an approximately north–south-trending fault zone of about 4–7 km width and 36 km length. It is composed of a number of parallel to obliquely oriented faults with considerable amounts of normal-slip component. Along the DFZ a number of strike-slip-induced morphotectonic features are present. These are the Yalaközü pull-apart basin, the Yalakçukurören pull-apart basin, alluvial fans, landslides and a number of historical ruins indirectly indicating historical activity of the DFZ (Fig. 4d and e; Emre *et al.* 2000).

Adıyaman *et al.* (2001) reported that the age of the same fault, named the Orta Fault, is Middle Miocene or older because it is covered by middle Miocene sediments of the Çerkeş–Kurşunlu–Ilgaz basin. Structural analysis of this fault (Adıyaman *et al.* 2001) has shown general west- to NW-dipping fault surfaces with left-lateral slip in the Early–Middle Miocene and dominantly normal slip in the Late Miocene–Plio-Quaternary (Fig. 4b and c). Kaymakçı *et al.* (2003) reported that the Eldivan Fault Zone (EFZ) is a sinistral strike-slip fault zone with a reverse component, and has resulted from reactivation of a Neotethyan suture zone that dips NW, and the reverse nature of the EFZ is due to the palaeotectonic nature of the fault zone. Palaeostress patterns constructed by Kaymakçı *et al.* (2000, 2003) indicate that the orientation of major principal stress (σ_1) is consistently NW–SE whereas the intermediate stress is vertical, indicating strike-slip deformation in the region.

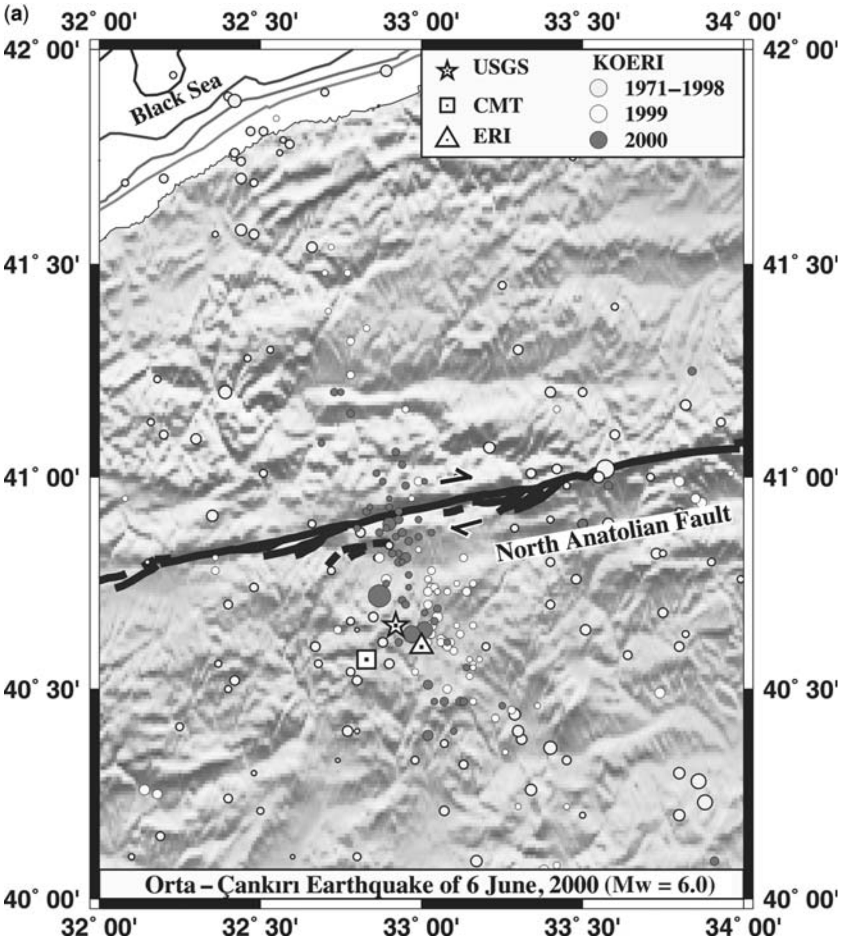

Fig. 5. (**a**) Regional seismicity in the central segment of North Anatolian Fault (NAF; mapped by Şaroğlu *et al.* 1987) during 1971–2000 for M >2, with aftershock data after Kandilli Observatory. Star, square and triangle indicate the instrumental epicentres of the 6 June 2000 Orta–Çankırı earthquake reported by the USGS, Harvard-CMT and ERI, respectively. GTOPO-30 global topography data are from the USGS and re-sampled at 0.1 min. Bathymetry data are from Smith & Sandwell (1997). (**b**) Lower hemisphere projections of the focal mechanisms corresponding to the minimum misfit solutions of earthquakes studied here and by earlier workers (see Table 1 for details). Compressional quadrants are shaded. Numbers in dilatational quadrants identify the focal depths obtained from the inversion.

Earthquake source parameters from inversion of teleseismic body-waveforms

Data reduction

We used both P- and SH-waveforms and first-motion polarities of P-waves to constrain earthquake source parameters. The approach we followed is that described by Taymaz *et al.* (1990, 1991*a*, *b*) to study earthquakes in the Hellenic trench, the Aegean region and on the East Anatolian Fault Zone (EAFZ), respectively. We compared the shapes and amplitudes of long-period P- and SH-waveforms recorded by GDSN stations in the distance range 30–90° with synthetic waveforms. To determine source parameters we used the McCaffrey & Abers (1988) version of Nábělek's (1984) inversion procedure, which minimizes, in a weighted least-squares sense, the misfit between observed and synthetic seismograms (McCaffrey & Nábělek 1987; Nelson *et al.* 1987; Fredrich *et al.* 1988). Seismograms are generated by combining direct (P or S) and reflected (pP and sP, or sS) phases from a point source embedded in a given velocity structure. Receiver structures are assumed to be homogeneous half-spaces. Amplitudes are adjusted for geometric spreading, and for attenuation using Futterman's (1962) operator, with $t^* = 1$s for P and $t^* = 4$ s for SH. As explained by Fredrich *et al.* (1988), uncertainties in t^* affect mainly source duration and seismic moment, rather than source orientation or centroid depth. Seismograms were weighted according to the azimuthal distribution of stations, such that stations clustered together were given smaller weights than those of isolated stations (McCaffrey & Abers 1988). The inversion routine then adjusts the strike, dip, rake, centroid depth and source time

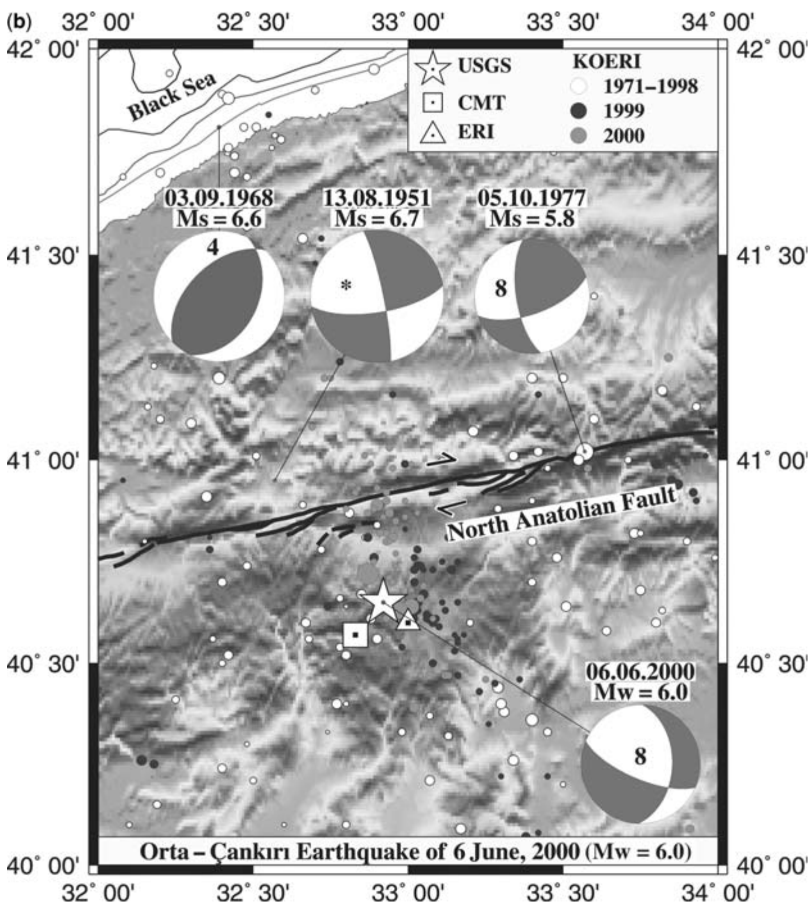

Fig. 5. *Continued.*

function, which is described by a series of overlapping isosceles triangles (Nábělek 1984) whose number and duration we selected.

Our experience with the inversion routine was very similar to that of Nelson *et al.* (1987), McCaffrey (1988), Fredrich *et al.* (1988) and Molnar & Lyon-Caen (1989). We found that a point source, in which all slip occurs at the same point (the centroid) in space but not in time, was a good approximation; that is, we saw no indication of systematic azimuthal variations in waveforms that might be associated with rupture propagation. However, the waveforms show evidence of multiple ruptures that we attempted to match by later sub-events that are discussed in greater detail below. The focal sphere was generally covered by observations in all quadrants, although with more stations to the north than the south, and we found that estimates of the strike, dip, rake and centroid depth were relatively independent of each other. Thus if one parameter was fixed at a value within a few degrees or kilometres of its value yielded by the minimum misfit of observed and synthetic seismograms, the inversion routine usually returned values for the other parameters that were close to those of the minimum misfit solution. The strikes and dips of nodal planes were consistent, within a few degrees, with virtually all first-motion polarities (Figs 5–8). The estimate of seismic moment clearly depended on the duration of the source time function, and to some extent on centroid depth and velocity structure. As our main interest is in source orientation and depth, we did not concern ourselves much with uncertainties in seismic moment, which in most cases is probably about 30%. We estimated the lengths of the time functions by increasing the number of isosceles triangles until the amplitudes of the later ones became insignificant. The seismogram lengths we selected for inversion were sufficient to include the reflected phases pP, sP and sS. We examined the P-waves for PcP arrivals, where they were anticipated within the selected window, but this phase was never of significant amplitude. ScS presented a greater problem, and we generally truncated our inversion window for SH-waves before the ScS arrival. The source velocity structures we used to calculate the synthetic seismograms are those reported by Jeffreys & Bullen (1940) and the IASPE91 (Lee 1991) Earth models. We assumed the centroid was in a layer with P velocity 6.5 km s^{-1}, which is a likely lower crustal velocity (Makris & Stobbe 1984) and appropriate for calculating the take-off angles of ray paths leaving the source. Uncertainty in the average velocity above the source leads directly to an uncertainty in centroid depth, which we estimate to be about ± 2 km for the range of depths involved in this study.

Uncertainties in source parameters

Having found a set of acceptable source parameters, we followed the procedure described by McCaffrey & Nábělek (1987), Nelson *et al.* (1987), Fredrich *et al.* (1988), Taymaz *et al.* (1990, 1991*a*, *b*), and Taymaz & Price (1992), in which the inversion routine is used to carry out experiments to test how well individual source parameters are resolved. We investigated one parameter at a time by fixing it at a series of values to either side of its value yielded by the minimum misfit solution, and allowing the other parameters to be found by the inversion routine. We then visually examined the quality of fit between observed and synthetic seismograms to see whether it had deteriorated from the minimum misfit solution. In this way we were able to estimate the uncertainty in strike, dip, rake and depth for each event. In common with the researchers cited above, we believe that this procedure gives a more realistic quantification of likely errors than the formal errors derived from the covariance matrix of the solution. We found that changing the depth of this earthquake by more than 2–3 km produced a noticeable degradation in the fit of waveforms, and take this to be a realistic estimate of the uncertainty in focal depth. This estimate, which is listed in Table 1, does not include the uncertainty related to the unknown average velocity above the source, discussed above. These tests give us some confidence

Fig. 6. This (and subsequent similar figures) shows the radiation patterns and synthetic waveforms for the minimum misfit solution returned by the inversion routine, as well as the observed waveforms. Continuous lines are observed waveforms, and the inversion window is identified by a short vertical bar. Dashed lines indicate synthetic waveforms. For the purposes of display, waveform amplitudes have been normalized to that of an instrument with a gain of 6000 at a distance of 60°. The station code is shown to the left of each waveform, together with an upper-case letter that identifies its position on the focal sphere and a lower-case letter that identifies the type of instrument (d, GDSN long-period). The vertical bar beneath the focal spheres shows the scale in microns, with the lower-case letter identifying the instrument type as before. The source time function is shown in the middle of the figure, and beneath it is the time scale used for the waveforms. Focal spheres are shown with P and SH nodal planes, in lower hemisphere projection. Station positions are indicated by letter, and are arranged alphabetically clockwise, starting from north. ●, ○, P- and T-axes, respectively. Beneath the header at the top of the figure, which shows the date, body-wave and surface-wave magnitudes, are given the strike, dip, rake, centroid depth and seismic moment (in units of $\times 10^{18}$ N m) of the minimum misfit solution obtained from the inversion of teleseismic long-period P and S body waveforms.

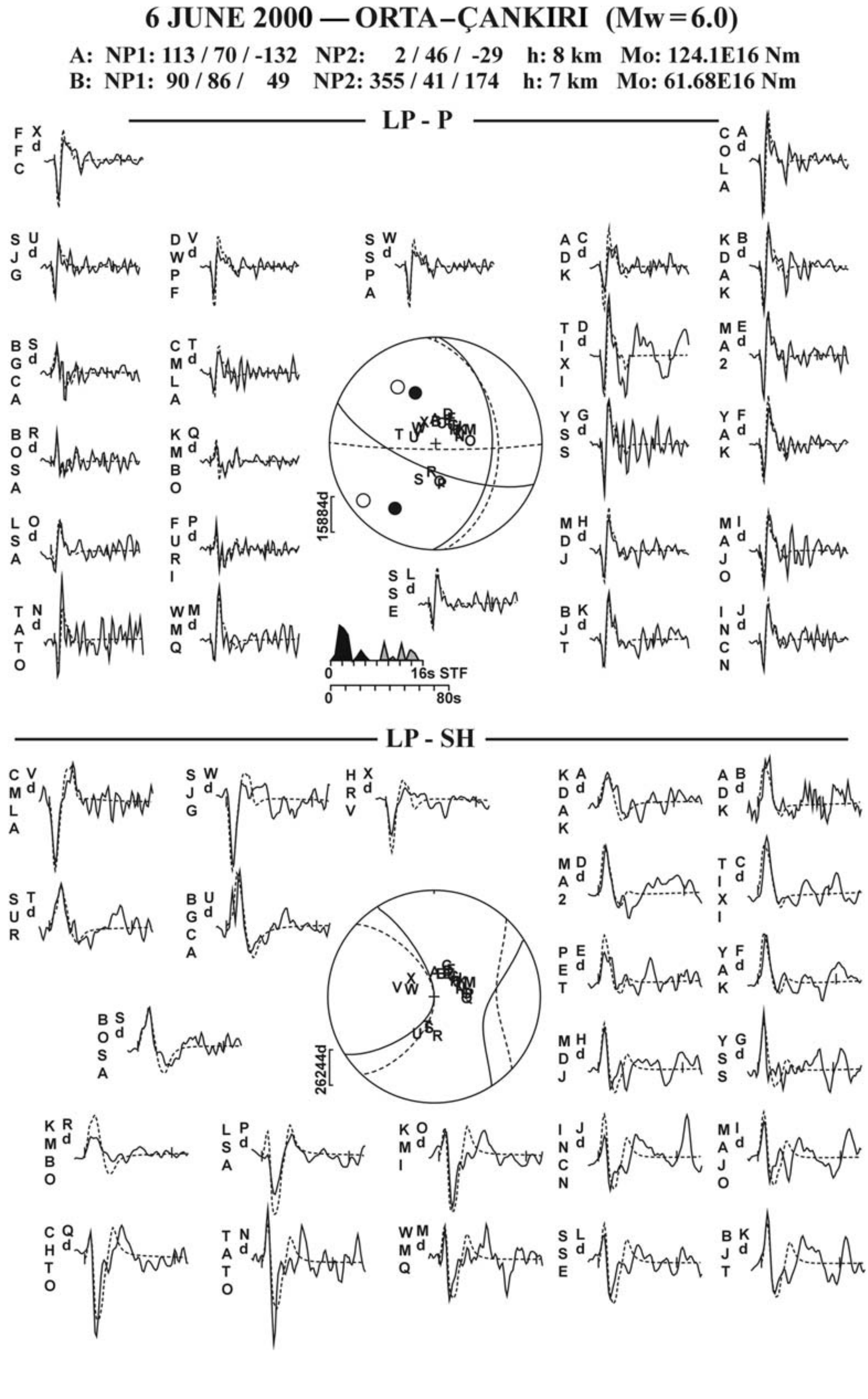
6 JUNE 2000 — ORTA–ÇANKIRI (Mw=6.0)
A: NP1: 113 / 70 / -132 NP2: 2 / 46 / -29 h: 8 km Mo: 124.1E16 Nm
B: NP1: 90 / 86 / 49 NP2: 355 / 41 / 174 h: 7 km Mo: 61.68E16 Nm
LP - P
15884d
0
16s STF
0
80s
LP - SH
26244d

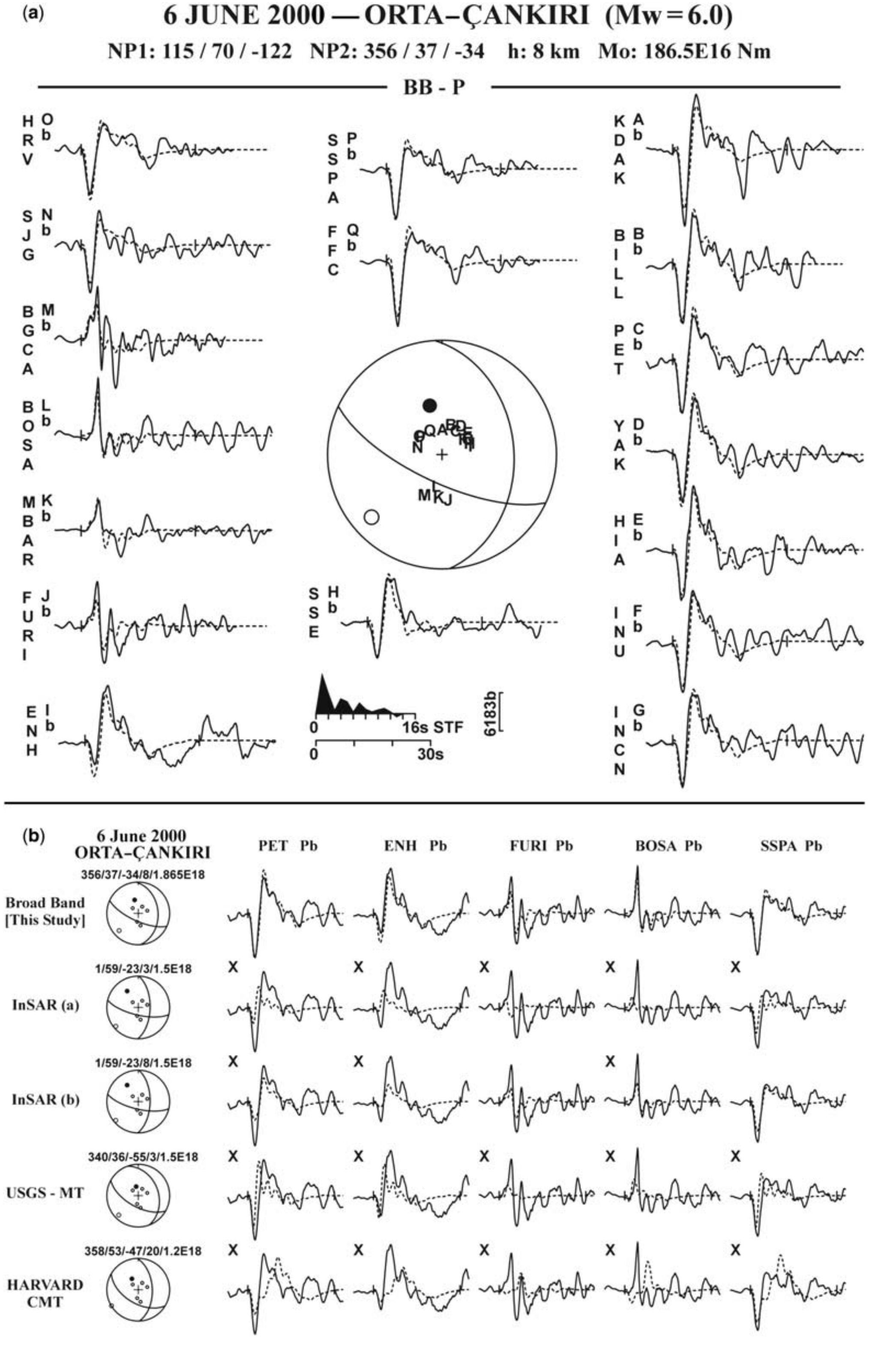
(a)
6 JUNE 2000 — ORTA–ÇANKIRI (Mw = 6.0)
NP1: 115 / 70 / -122 NP2: 356 / 37 / -34 h: 8 km Mo: 186.5E16 Nm
BB - P
HRV O b
SJG N b
BGCA M b
BOSA L b
MBAR K b
FURI J b
ENH I b
SSPA P b
FFC Q b
SSE H b
KDAK A b
BILL B b
PET C b
YAK D b
HIA E b
INU F b
INCN G b
0
16s STF
0
30s
6183b
(b)
6 June 2000
ORTA–ÇANKIRI
356/37/-34/8/1.865E18
Broad Band [This Study]
1/59/-23/3/1.5E18
InSAR (a)
1/59/-23/8/1.5E18
InSAR (b)
340/36/-55/3/1.5E18
USGS - MT
358/53/-47/20/1.2E18
HARVARD CMT
PET Pb
ENH Pb
FURI Pb
BOSA Pb
SSPA Pb
X

that there is no significant trade-off between source parameters for this event. The greatest change occurs to the value of seismic moment, which varies by 20%.

The pattern of focal mechanisms

Aftershock distributions

Figure 5 shows the background seismicity and aftershock distributions of the 6 June 2000 Orta–Çankırı sequence reported by KOERI, using P-wave arrival times picked at regional stations by station operators. The aftershocks, which occur in a broad zone elongated north–south to NW–SE, are subparallel to the trend of the major faults in the region (Fig. 4d and e, Emre *et al.* 2000), but lie to the east of the macroseismic epicentre for the main shock. The USGS, Harvard-CMT, ERI and KOERI locations of the Orta earthquake lie about 10–15 km west of the macroseismic epicentre. It is likely that the locations for earthquakes the size of the Orta earthquake may be as much as 15–20 km in error (Taymaz *et al.* 1991; Taymaz & Price 1992). The influence of station distribution is also significant for the mislocation vectors, which are similar to that for J–B times, as reported by Kennett & Engdahl (1991). Their study showed a systematic shift of ISC locations in the Aegean.

Focal mechanisms in this area for earthquakes larger than Ms = 5.8 since 1960 were determined using the same inversion algorithm and procedure (Fig. 5b). Two types of mechanism are common: strike-slip faulting with roughly east–west nodal planes and normal faulting with nodal planes trending NNW–SSE. Most of the strike-slip solutions are near the NAFZ, whereas the normal faulting solution of the Orta–Çankırı earthquake is on the nearby secondary faults. The one obvious anomaly is the high-angle reverse faulting solution of the 3 September 1968 Bartın earthquake (Fig. 5b and Table 1) in NW Turkey, which shows shortening in a roughly NW–SE direction. All of solutions are well constrained by first-motion polarities and waveforms (Özay 1996; Tan 1996).

The 6 June 2000 Orta–Çankırı earthquake was the largest instrumentally recorded event occurred we were able to study (Table 1; Taymaz & Tan 2001; Taymaz *et al.* 2002*a*), with a moment of $M_o = 1.85 \times 10^{18}$ N m. It occurred close to a restraining bend in the north–south-striking right-lateral strike-slip fault that moved in the much larger earthquake of 13 August 1951 (McKenzie 1972). It is further obvious for small earthquakes, particularly aftershocks, to have mechanisms incompatible with a uniform regional strain field (e.g. Richens *et al.* 1987), but unusual to see this effect with earthquakes large enough to study teleseismically. Hence, the faulting in this anomalous earthquake could be related to the local geometry of the main strike-slip system, and may not be a reliable guide to the regional strain field in central Turkey.

Teleseismic body waveforms

Long-period P, SH and broadband P waveforms at teleseismic distances were clearly recorded for this earthquake. Thus in Figures 6–8 we have compared the observed body-wave seismograms with synthetics generated following the procedure described by Taymaz *et al.* (1991*a*, *b*) and Taymaz & Price (1992), among many others.

Long-period P and SH body waveforms

The minimum misfit solution for the earthquake of 6 June 2000 is shown in Figures 6–8. The nodal planes of this solution are compatible with virtually all first-motion P polarities, shown in Figure 8b. The P and SH pulses are simple at all azimuths and characteristic of normal faulting with a shallow focal depth. There is good coverage of the focal sphere at all azimuths, for both first-motion and long-period P, SH and broadband P waveform data. We carried out many experiments as described by McCaffrey & Nábělek (1987),

Fig. 7. (**a**) Minimum misfit solution for the broadband P waveforms. For the purposes of display, waveform amplitudes have been normalized to that of an instrument with a gain of 3000 at a distance of 70°. The remainder of the display convention is as in Figure 6. (**b**) A selection of waveforms from a run of the inversion program. The top row shows waveforms from the minimum misfit solution. The stations are identified at the top of each column, with type of waveform marked by P and followed by the instrument type (b, broadband). At the start of each row the P focal sphere is shown for the focal parameters represented by the five numbers (strike, dip, rake, depth and moment), showing the positions on the focal spheres of the stations chosen. The convention for the waveforms is as in Figures 6 and 7, but here the large × shows matches of observed to synthetic waveforms that are worse than in the minimum misfit solution. We compare selected waveforms from misfit solution (a) with those generated by sources with orientations of the InSAR obtained in the present study, and reported USGS-MT and Harvard-CMT solutions. In the following rows the strike, dip, rake, depth and moment were fixed at the values of InSAR, USGS-MT and Harvard-CMT modelling results (see Table 2).

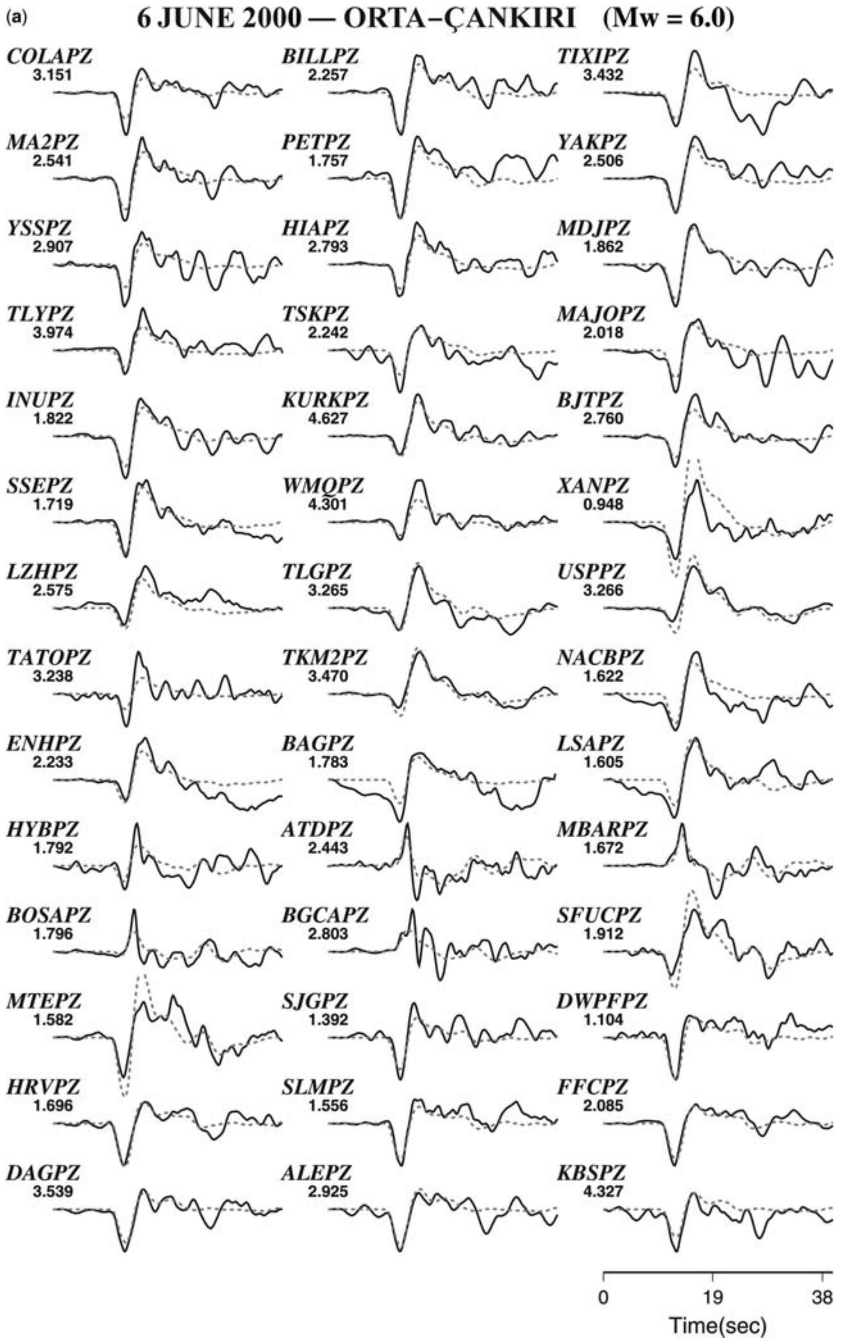

Fig. 8. (**a**) Comparison of the observed broadband P waveforms (continuous lines) with the synthetic waveforms (dashed lines) used in rupture history and slip distribution analyses. The numbers below the station code indicate maximum amplitude, and the time scale is shown below the figure. (**b**) Lower hemisphere equal area projections of the first-motion polarity data. Station positions of the focal sphere have been plotted using the same velocity below source (6.5 km s^{-1}) that was used in our waveform inversion procedure. ●, compressional first motions, ○, dilatational; all were read on long-period, short-period and broadband instruments of the GDSN, when available. Nodal planes are those of the minimum misfit solutions. Beneath the selected waveforms, marked with station codes, at the bottom of the figure is given the event's header (month, date, year, geographical location), with both of the nodal planes that illustrate the strike, dip and rake of the minimum solution. ■, □, P- and T-axis, respectively.

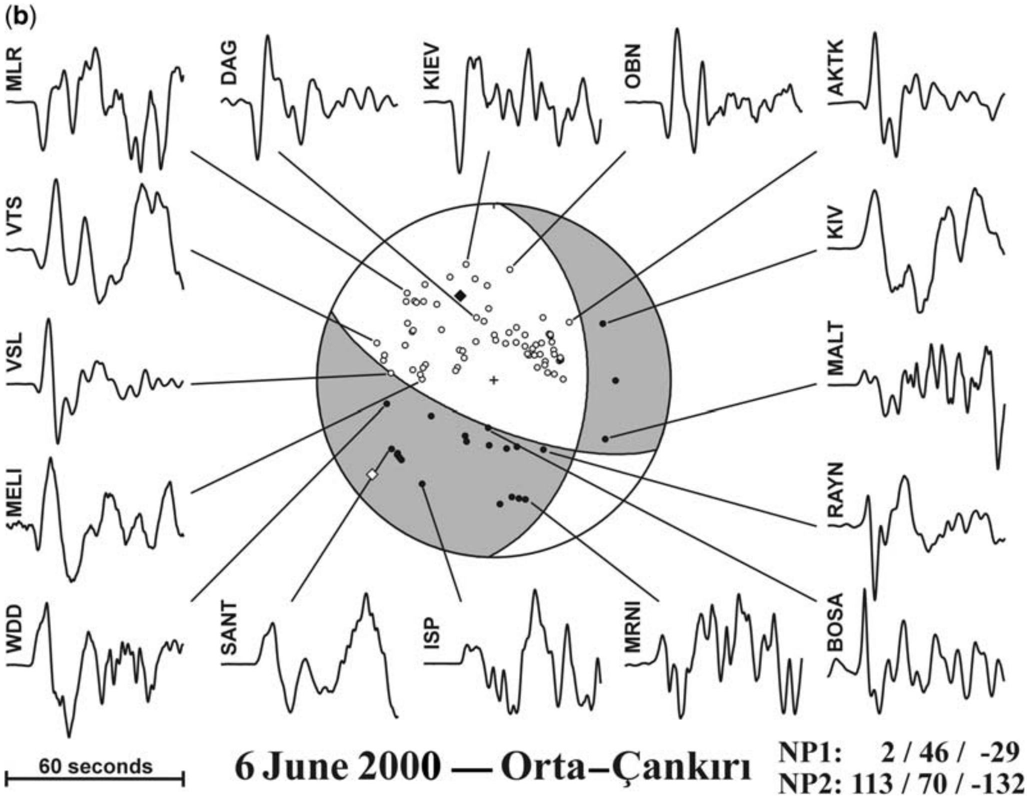

Fig. 8. *Continued.*

Nelson *et al.* (1987), Taymaz *et al.* (1990, 1991*a*, *b*), Taymaz & Price (1992) and Taymaz (1993), in which the inversion routine is used to carry out experiments to test how well individual source parameters resolved, and based on these, estimate the source parameters and uncertainties of the 6 June 2000 Orta–Çankırı earthquake to be: Nodal Plane 1: strike $2 \pm 5°$, dip $46° \pm 5°$; rake $-29 \pm 5°$; Nodal Plane 2: strike 113°, dip 70°; rake −132°; principle axes: P = 338 (48); T = 232 (14); B = 131 (39); depth 8 ± 2 km (although this does not include uncertainty related to velocity structure), and seismic moment (M_o) in the range of (140–185) $\times 10^{16}$ N m.

In Figure 7b, we compare, at selected stations, the waveforms from the minimum misfit solution with those from some of the other reported solutions. The strike, dip, rake, depth and moment were fixed using the values of InSAR, USGS-MT and Harvard-CMT reported results (see Table 2). The minimum misfit solution obtained from joint inversion of long-period P, SH and broadband P waveform data is clearly much better constrained than that of InSAR modelling results, which produces a poor fit (marked with $\times$) of the seismograms at several stations (Fig. 7b, rows 2 and 3). In rows 2 and 3, InSAR parameters (see Table 2) are used, and the only difference is the focal depth, which was fixed at values of 3 and 8 km to test the lower and upper limits, respectively. The InSAR solution obtained in the present study differs from the body-wave modelling results by 5° in strike, 22° in dip, and 11° in rake. The differences in dip, rake and depth are marginally outside the acceptable errors of body-wave solutions (Tables 1 and 2). In rows 4 and 5 of Figure 7b we fixed the source orientation using USGS-MT and Harvard-CMT reported solutions. The fit of waveforms is noticeably worse than in the minimum misfit solution, and the polarities are incorrect (Fig. 7b).

Rupture history and slip distribution inversion of broadband P body waveforms

In recent years there has been significant progress in our understanding of the nature of earthquakes and Earth structure, mainly as a result of our improved ability to interpret broadband seismograms

Table 1. *Source parameters of earthquakes shown in Figures 4–6*

Origin time, t_0 (GMT)	Latitude (°N)	Longitude (°E)	M_w	Nodal Plane 1			Nodal Plane 2			Focal depth (km)	Seismic moment ($\times 10^{16}$ Nm)	STF duration $\Delta\tau_{95}$(s)
				Strike (°)	Dip (°)	Rake (°)	Strike (°)	Dip (°)	Rake (°)			
13 August 1951 Çerkeş (McKenzie 1972)												
18:33:30.0	40.95	32.57	6.7	81	70	−172	348	82	−20	–	–	–
3 September 1968 Bartın (Tan 1996)												
08:19:52.0	41.81	32.39	6.3	26	40	75	255	52	102	4	400	*c*. 14
5 October 1977 Kurşunlu (Özay 1996)												
05:34:43.0	41.02	33.57	5.8	70	65	155	171	67	27	8	58	*c*. 6
6 June 2000 Orta–Çankırı (this study)												
02:41:53.2	40.70	32.98	6.0									
InSAR				1	59	−23	–	–	–	3–8	150	–
Broadband P-waves				356	37	−34	115	70	−122	8	186	*c*. 15
Long-period P- and SH-waves and rupture or slip distribution				2	46	−29	113	70	−132	6–8	140–185	*c*. 16
							Fault rupture area: *c*. 42 km^2; stress drop: 128 bar					
							Maximum and average slip: *c*. 231 cm, *c*. 111 cm					

The detailed source parameters of the Orta–Çankırı earthquake are obtained from inversion of teleseismic P and SH body waveforms and InSAR data with rupture history (slip distribution). STF, Source Time Function (in seconds).

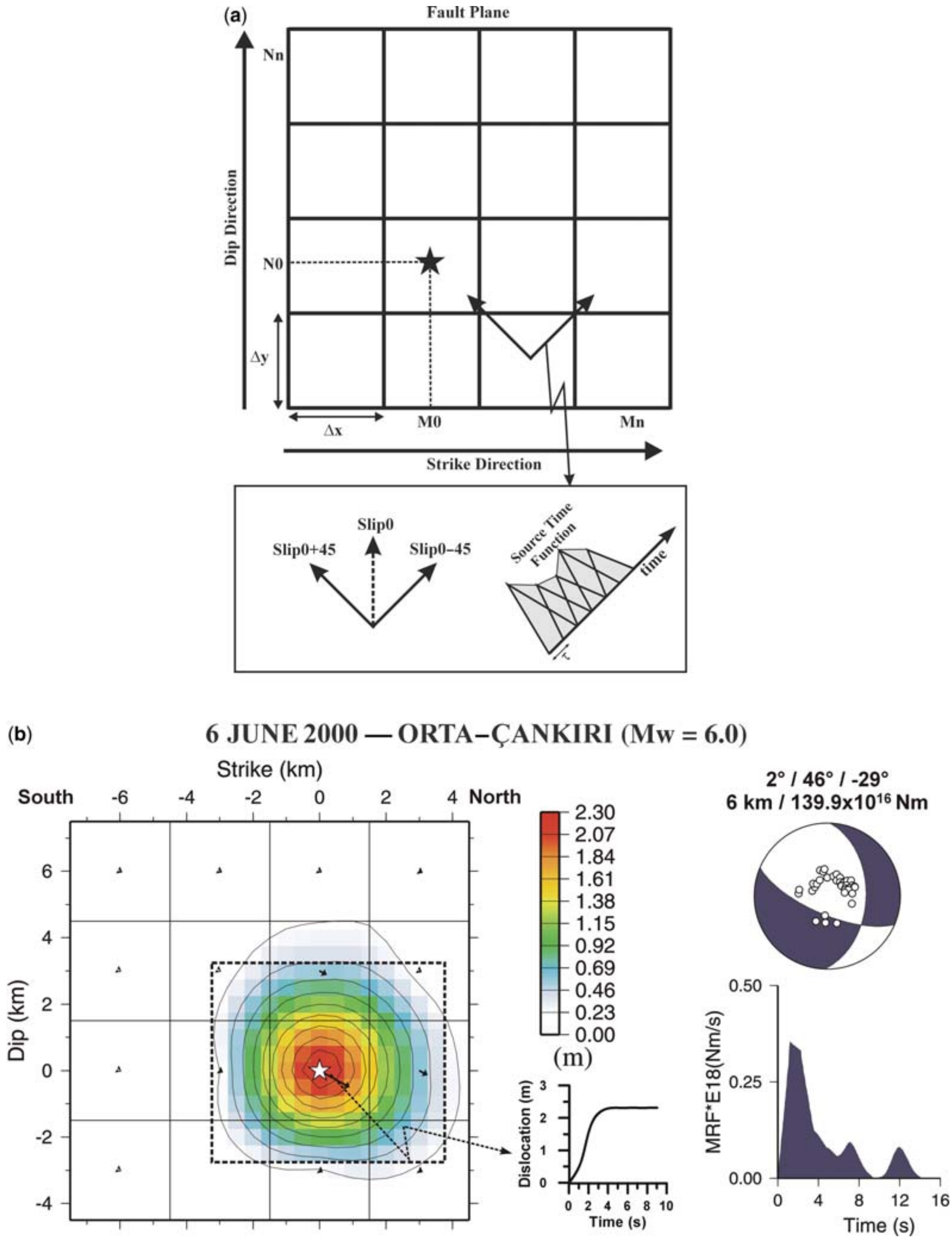

Fig. 9. (**a**) Schematic diagram summarizing the source expression during the rupture process. The fault plane is divided into sub-faults whose numbers (Nn), and dimensions (Δx–Δy) are predefined along the strike and dip on the fault plane. Also shown are the two components of slip vector with rakes (slip 0 $\pm$ 45), and parameterized moment-rate (source-time) function, which is described by the amplitudes of a series of overlapping isosceles triangles (Nábělek 1984; Yagi & Kikuchi 2000) whose numbers and duration were determined during the inversion procedure. (**b**) The rupture history obtained from our joint inversion of teleseismic P and SH long-period and broadband body waveforms. Earthquake focal mechanism, total moment rate function (source-time function), and distribution of coseismic slip are shown. The star indicates the location of the rupture initiation (initial break) located at a depth of about 6 km (0 km$\times$0 km). The slip vectors and the distribution of slip magnitudes are also presented.

Table 2. *Source parameters of the Orta–Çankırı earthquake from InSAR and seismology*

	HRV CMT	USGS MT	InSAR
Scarp latitude (°N)	40.57	40.62	$40.63 \pm 0.01^*$
Scarp longitude (°E)	32.83	32.97	$32.96 \pm 0.01^*$
Length (km)	–	–	9 ± 1
$M_0(10^{16}$ N m)	120	150	$150 \pm 40^\dagger$
Slip (m)	–	–	1(fixed)‡
Strike§	358°/121°	340°/122°	$1 \pm 7°$
Dip§	53°/54°	36°/69°	$59 \pm 10°$
Rake§	−47°/−132°	−55°/−106°	$-23 \pm 8°$
Depth (km)	20.5	3	3.2 ± 0.6–$7.7 \pm 1.9^\ddagger$
l.o.s. offset (mm)	–	–	-13.6 ± 6

InSAR data are from the present study. Error bounds of 1σ are given for the InSAR fault parameters.
*Location of surface scrap, projected up-dip from the centroid location.
†Assuming Lamé elastic constants $\mu = 3.23 \times 10^{10}$ Pa and $\lambda = 3.23 \times 10^{10}$ Pa.
‡Slip trades-off with depth extent of faulting. If a 1 m slip is chosen then the best-fit depth range is 3.2–7.7 km.
§The two numbers for the seismological solutions are the two nodal planes of the focal mechanisms reported.
l.o.s., line of sight.

recorded globally after major earthquakes. Kikuchi & Kanamori (1991) developed a procedure to determine the detailed source rupture processes, which provide valuable information on the nature of Earth dynamics (plate interactions, etc.), and this has recently been improved by Yoshida *et al.* (1996), Yagi & Kikuchi (2000) and Yagi (2002), among many others. The results contain valuable information, which is also related to strong ground motion experienced at the vicinity of faults. Yagi & Kikuchi (2000) expressed the rupture process as a spatio-temporal slip distribution on the fault plane (see Fig. 9 for details).

We followed the procedure developed by Yagi and Kikuchi (2000), and retrieved 42 teleseismic broadband P- body-wave data that were band-pass filtered between 0.01 and 1 Hz, and converted into ground displacement with a sampling time of 0.2 s (Fig. 8a). We have further introduced time corrections using the standard Jeffreys & Bullen (1940) crustal structure so that the observed P arrivals coincide with the theoretical arrival time of P-waves. We determined the spatio-temporal distribution of fault slip by applying a multi-time window inversion to the data obtained. Then, we resolved their relative weight so that the standard deviations of the teleseismic P-wave is about 10% of their individual maximum amplitudes by analysing the quality of observed records and background noise level. We assumed that faulting occurs on a single fault plane and that the slip angle is unchanged during the rupture. There is good coverage of the focal sphere at all azimuths, for both waveform (Fig. 8a) and first-motion (Fig. 8b) data. The waveform inversion provides us with direct information about the extent of the coseismic rupture area. Thus, to obtain the detailed rupture history, first we selected a fault area of 12 km × 12 km to obtain a rough estimate of the rupture area (Fig. 8a and b), which we divided into 4 × 4 sub-faults, each with an area of 3 km × 3 km. The source-time (slip-rate) function of each sub-fault is expanded in a series of 10 triangle functions with a rise time (τ), of 1.2 s. A rupture front velocity (*Vr*) is set at 2.8 km s^{-1} (for further information, see Hartzell & Heaton 1983; Lay & Wallace 1995; Ide & Takeo 1997; Imanishi *et al.* 2004), which gives the start time of the base function at each sub-fault. The inversion results are given in Figures 8 and 9, and Table 1. Figure 9b shows the final dislocation distribution. The source rupture process is rather simple and characteristic of a shallow crustal normal faulting.

We estimate the source parameters and uncertainties of the 6 June 2000 Orta–Çankırı earthquake from rupture history analyses to be: Nodal Plane 1: strike $2 \pm 5°$, dip $46° \pm 5°$; rake $-29 \pm 5°$; Nodal Plane 2: strike 113°, dip 70°; rake −132°; depth 6 ± 2 km (although this does not include uncertainty related to velocity structure, and is nearly constant along the fault strike), and seismic moment, $M_o = 140 \times 10^{16}$ N m (Mw 6.0). There is only one asperity recovered on the fault plane and the rupture is localized and estimated to propagate evenly in NE–SW direction with a slip vector of 203°. The largest slip of 2.31 m occurred at a depth of 6 km in the first 3 s of source rupture history (Fig. 9b). We have estimated the effective rupture area, stress drop ($\Delta\sigma = 2.5 \times M_o/S^{1.5}$, where S is the area of the maximum slip of 2.31 m, 6×7 km^2), maximum slip and average slip to be *c.* 42 km^2, 128 bar, 231 cm and 111 cm, respectively. The total source duration is *c.* 16 s.

Earthquake source parameters from InSAR

In recent years, synthetic aperture radar interferometry (InSAR) has been established as a valuable technique with which to measure the surface deformation caused by earthquakes (Massonet *et al.* 1993; Zebker *et al.* 1994; Feigl *et al.* 1995; Wright 2002). By differencing the phase of the ground returns from an area, illuminated on repeated occasions by a SAR carried on an orbiting satellite, detailed maps of crustal deformation can be obtained with a spatial resolution of a few tens of metres and a measurement precision of a few millimetres. Further details on the technique have been given in reviews by Massonet & Feigl (1998) and Bürgmann *et al.* (2000). We use data from the ERS-2 SAR, which has a wavelength of 56 mm (C-band). Each interference 'fringe' corresponds to 28 mm of range change (the component of displacement in the satellite line of sight, 23º from the vertical at the scene centre).

InSAR data

Only limited SAR data were available for the Orta–Çankırı earthquake (Taymaz *et al.* 2002*a*). The best coseismic pair had an altitude of ambiguity of *c*. 270 m and a temporal separation of 10 months, only 5 days of which were after the earthquake (ERS-2, track 479, frame 2786, orbits 22878 (5 September 1999) and 26886 (11 June 2000)). The interferogram was processed using the ROI_pac software, and a 3 arcsecond (*c*. 90 m) digital elevation model (DEM) from the US Department of Defense was used to make the topographic correction. The altitude of ambiguity is the magnitude of topographic error that will cause a single interference fringe of erroneous phase. In this case, the DEM is thought to have height errors of less than 50 m, corresponding to a phase error of *c*. 1.2 radians, or an error in range change of *c*. 5 mm. A nonlinear, power-spectrum filter (Goldstein & Werner 1998) was applied to the interferogram.

The resultant interferogram (Fig. 10) is mostly coherent and shows concentric fringes in the expected epicentral are. The fringe pattern is asymmetrical, with a pear-shaped pattern of about five concentric fringes of range (distance to satellite) increase in the south, and about two fringes of range decrease in the north. The interferogram's noise, mostly arising from changes in atmospheric conditions, can be assessed by examining the phase signal away from the epicentral area, where we do not expect any deformation. The range changes have an r.m.s. error of 14 mm. We also investigate spatial correlations of the InSAR noise, by determining the 1D covariance function (e.g. Hanssen 2001). The e-folding length scale of the InSAR noise for this interferogram is *c*. 6 km.

Inversion procedure

We use a hybrid Monte-Carlo, downhill simplex inversion procedure (Wright *et al.* 1999, 2001*a, b*) to determine the best-fitting model parameters. This procedure minimizes the misfit between our interferometric measurements of range change, sampled at discrete locations using the Quadtree Algorithm (e.g. Jónsson *et al.* 2002), and those predicted by a simple elastic dislocation model (Okada 1985). We solved for the nine parameters required to describe a single rectangular fault with uniform slip (strike, dip, rake, slip, latitude and longitude, fault length, minimum and maximum depth), as well as a line-of-sight offset and gradients in the x- and y-directions to account for orbital errors in the interferogram.

A posteriori errors to the best-fit fault parameters (Tables 1 and 2) were determined using a Monte-Carlo simulation technique (T.J. Wright pers. comm.). In this technique, 100 simulations of the InSAR noise, based on the 1D covariance function, are created. These are added to the original range change observations and each noisy dataset is inverted. The distribution of inverted parameters gives their error. The method also allows the trade-offs between parameters to be examined (Fig. 11).

Inversion results

The best-fit inversion solution comprises a nearly north–south fault plane, dipping *c*. 60º to the east, and with a combination of normal and left-lateral slip. Within error, this solution is in good agreement with the body-wave solution. The best-fit fault parameters were used to construct a model interferogram (Fig. 10c). This simple model reproduces the interferogram very well, as is evident by the lack of systematic misfit in the residual interferogram (Fig. 10d). The r.m.s. misfit is 8 mm, comparable with the level of atmospheric noise in the interferogram. Further complications to the model are therefore unnecessary. The geodetic moment of $(150 \pm 40) \times 10^{16}$ N m is also in good agreement with the estimate from body-wave modelling (Figs 6–9). One difficulty was that the fault slip trades-off strongly with the fault width for this inversion, such that large slips on narrow faults fit the data as well as lower slips on wider faults. To overcome this, we fixed the fault slip at 1 m, consistent with standard stress drops and slip to length ratios (e.g. Wells & Coppersmith 1994). This gives us a reasonable depth range of 3.2–7.7 km for this earthquake.

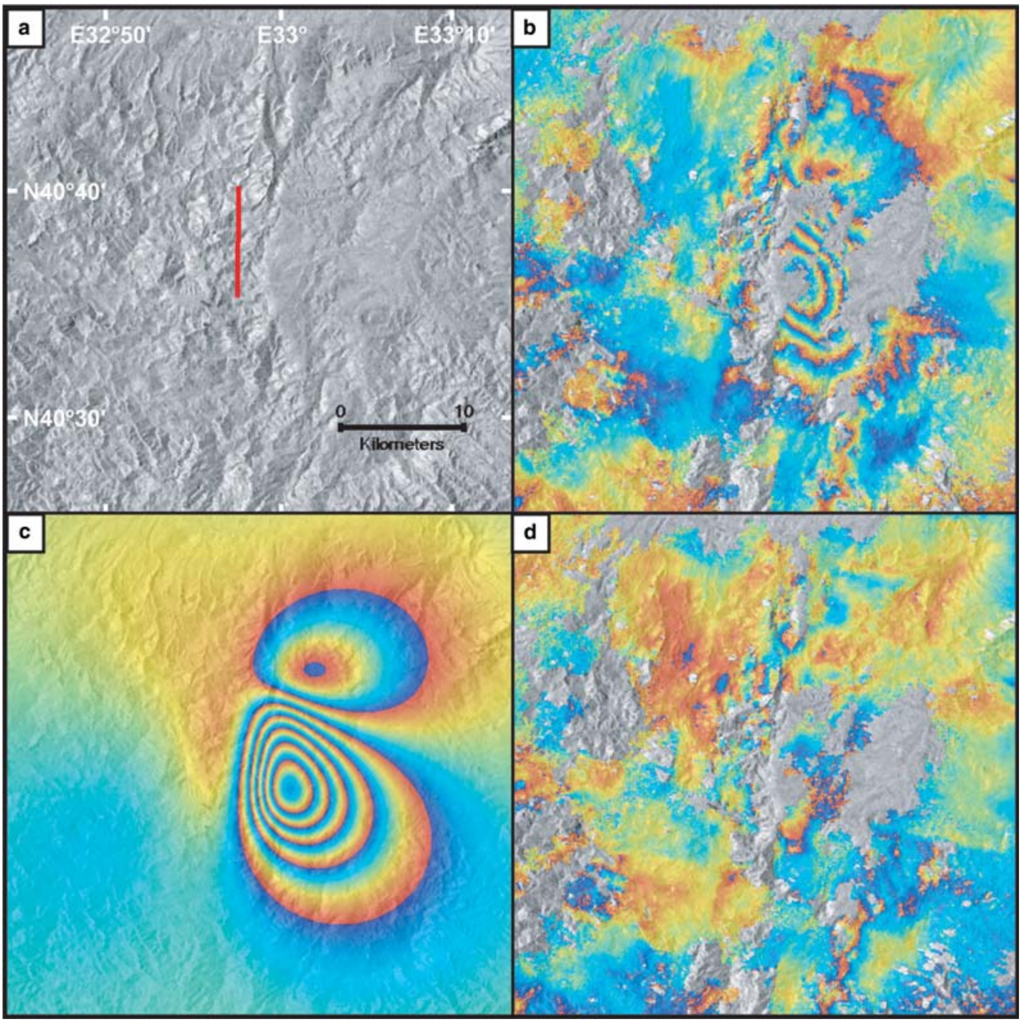

Fig. 10. Interferogram and model of the Orta–Çankırı earthquake. (**a**) SAR amplitude image, showing the location of the model surface rupture as a red line; (**b**) coseismic interferogram with a complete colour cycle of red through yellow to blue and back to red indicating an increase in range of 28 mm. Areas with no colour correspond to those where phase could not be unwrapped; (**c**) best-fit single-fault model, determined by inversion; (**d**) residual interferogram, obtained by subtracting (c) from (b).

We also investigated solutions that used the alternative (ESE–WNW-striking) nodal plane. Inversions in which the fault strike is held fixed at 113° (the strike determined from body-wave modelling) yield solutions that dip to the south at 70°, with a fault rake of −155°. The r.m.s. residual is 11 mm, larger than the 8 mm of the solution with a north–south-striking fault plane. Hence the north–south nodal plane is marginally preferred from the InSAR data alone. One surprising result of the inversion solution is that the best-fit slip was 7.7 ± 6 m. When combined with a very narrow best-fit depth range (4.8–5.3 km) this would give the earthquake an unusual aspect ratio, and abnormally high slip for an Mw = 6.0 earthquake (e.g. Wells & Coppersmith 1994). To determine if these values are well constrained by the InSAR data, we carried out a series of inversions, each time fixing the slip to a different value but solving for the best-fit depth range, with the fault geometry and rake held fixed. The result showed that these parameters trade-off against each other, such that for large values of slip, the depth range is small. For any value of slip equal to or greater than *c*. 1 m, the misfit and geodetic moment are approximately constant, but both increase sharply for lower

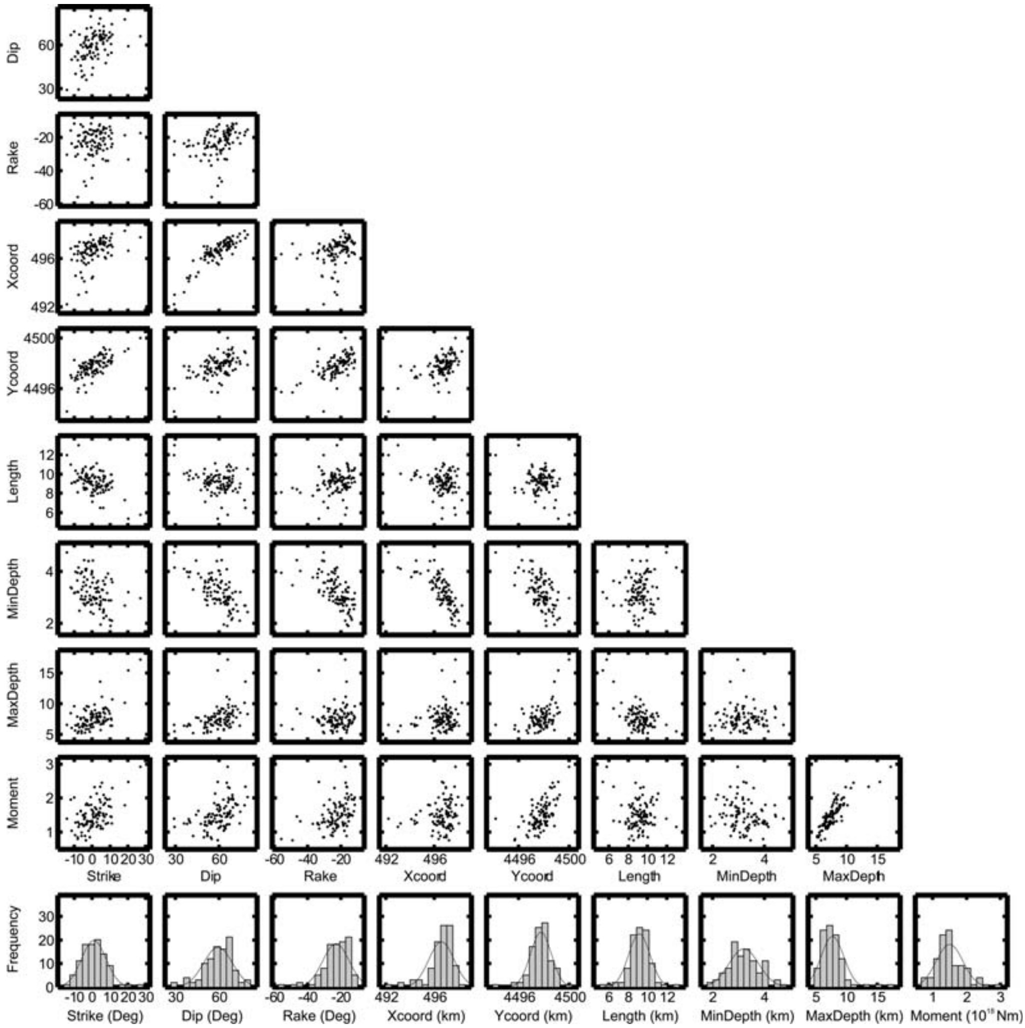

Fig. 11. Parameter trade-offs determined for the Orta–Çankırı earthquake using InSAR data. Each of the 100 dots in each figure is the solution of an inversion of the original InSAR data to which synthetic noise has been added. Histograms summarize the spread of solutions for each fault parameter, with the curves representing the Gaussian distributions with means and standard deviations as given in Table 2.

values of slip. The depth range found for a 1 m slip is more reasonable (3.6–7.4 km) and, given no additional constraints, these values are preferred. For very large values of slip, the depth range of the faulting becomes very small, and centred on a depth of 5 km.

Remote sensing data

One important factor that must be accounted for in seismotectonic studies is the site response caused by the surface conditions, the site effect. Earthquake damage may vary locally, being a function of the type of structures in the subsurface and/or soil mechanical ground conditions, such as faults and fractures, lithology or groundwater table. It has further been observed by macroseismic studies of topographic effects that in valleys and depressions damage intensity is higher because of higher earthquake vibration. These factors vary from earthquake to earthquake. Other influential factors are source distance and depth, azimuthal variation of source radiation, anelastic absorption and focusing effects of geological structures. Fault zones could cause constructive interference of multiple reflections

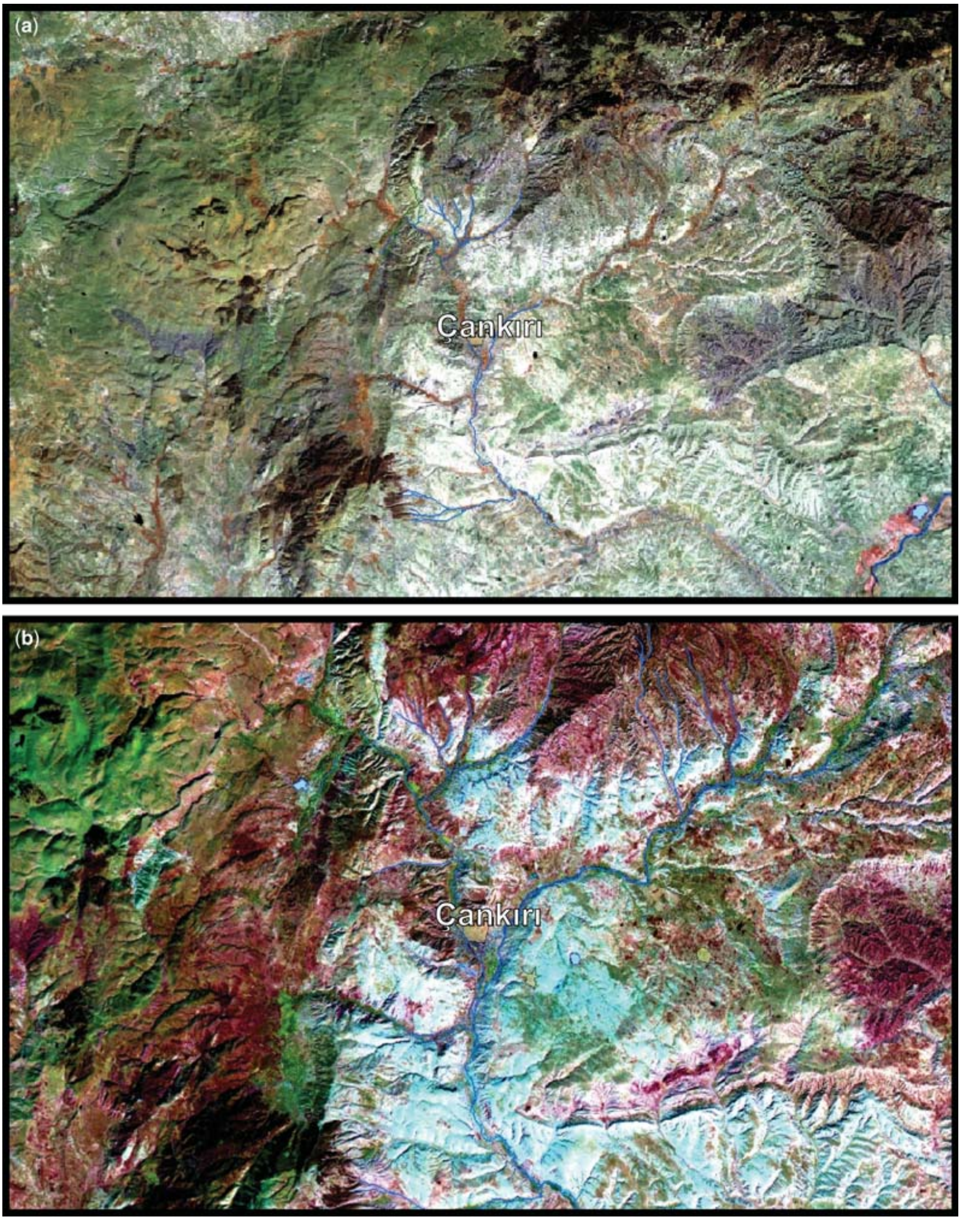

Fig. 12. (**a**) Digital elevation model (DEM) of the Orta–Çankırı region. LANDSAT ETM scene with HSV bands 4, 5, 3 and 8 is used. (**b**) LANDSAT ETM HSV image: bands 6, 5, 3 and 8 are used, and image resolution is 15 m. (**c**) DEM of North Anatolian Fault (NAF) at the Orta–Çankırı epicentre region.

of seismic waves at the boundaries between fault zones and surrounding rocks. Fault segments, their bends and intersection are the localized regions of stress concentration and seismic shock amplification. Intersecting fault zones could cause constructive interference of multiple reflections of seismic waves at the boundaries between fault zones and surrounding rocks. The

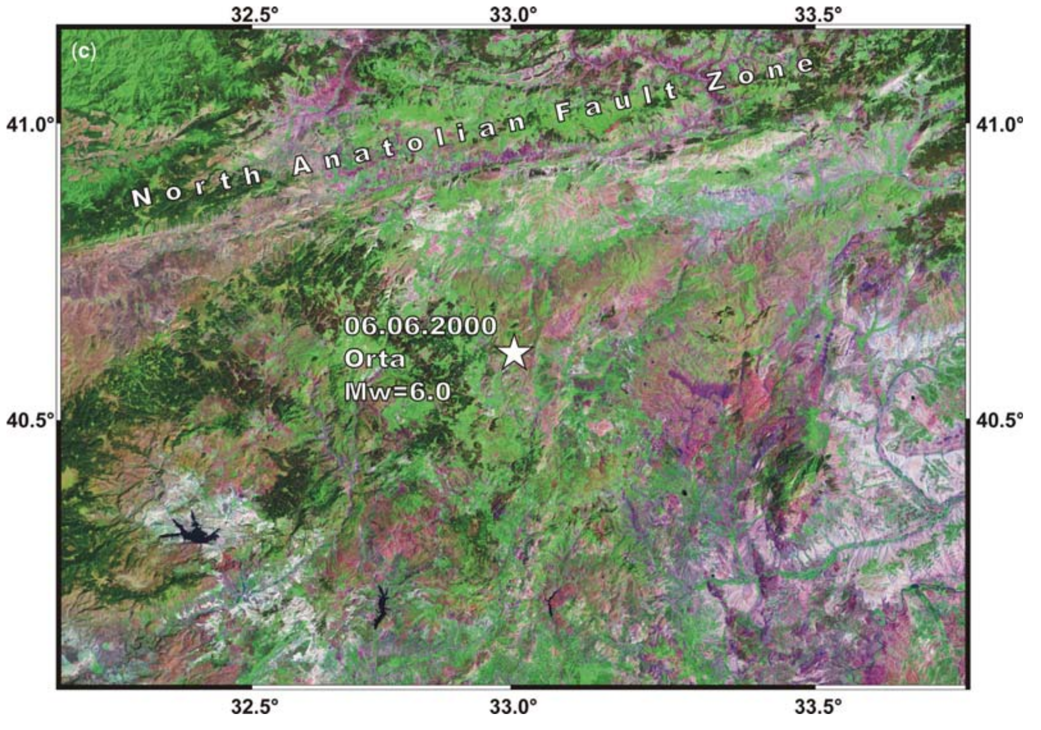

Fig. 12. *Continued.*

highest risk must be anticipated at the junctions of differently oriented ruptures, especially where one intersects the other. Compact fault zones consisting of distinct segments can be considered to be more dangerous in terms of seismic risk than those where active ruptures are scattered over a larger area. Those regions can be considered as being more exposed to earthquake shock as a result of amplification of guided seismic waves along crossing fault zones and soil amplification.

Therefore special attention is focused on precise mapping of traces of faults on satellite images, predominantly for areas with distinct expressed lineaments, as well as those with intersecting or overlapping lineaments or with unconsolidated sedimentary cover. Lineament analysis based on satellite images can help to delineate local fracture systems and faults that might influence seismic-wave propagation and influence the intensity of seismic shock. For example, merging lineament maps with isoseismal maps contributes to a better knowledge of subsurface structural influence on seismic shock intensity and on potentially earthquake-induced secondary effects such as landslides or soil liquefaction. Landslides cover a wide range including rock-fall, rockslide, debris slide and earth flow, and landslide risk high especially in steep slope areas. Landslides triggered by seismic shock have been documented in many parts of Turkey with existing slope instabilities. Subsurface fracture and fault patterns influence the shape and dimension of landslides to a large extent. Lineament analysis therefore provides important clues for delineation of areas prone to landslides, and especially a more precise localization of areas with a relatively high risk of slope failure.

Approach

For the present study LANDSAT 7 ETM images from northern central Turkey were obtained through the German Science Foundation (DFG, Bonn), the German Aerospace Centre (DLR, Oberpfaffenhofen) and EUROIMAGE (Rome). The LANDSAT ETM scene, LANDSAT 7 ETM, 29 May 1999, Track 177, Frame 32, was provided by EURIMAGE and DLR as Level 1G product (Fig. 12). This image product is radiometrically and geometrically corrected including output map projection and image orientation (UTM, WGS84), and resampled by using nearest neighbourhood algorithm. The LANDSAT data comprise six bands of multi-spectral data in the visible and IR portion of the spectrum. The image has a geometric resolution (30 m) that provides sufficient level of

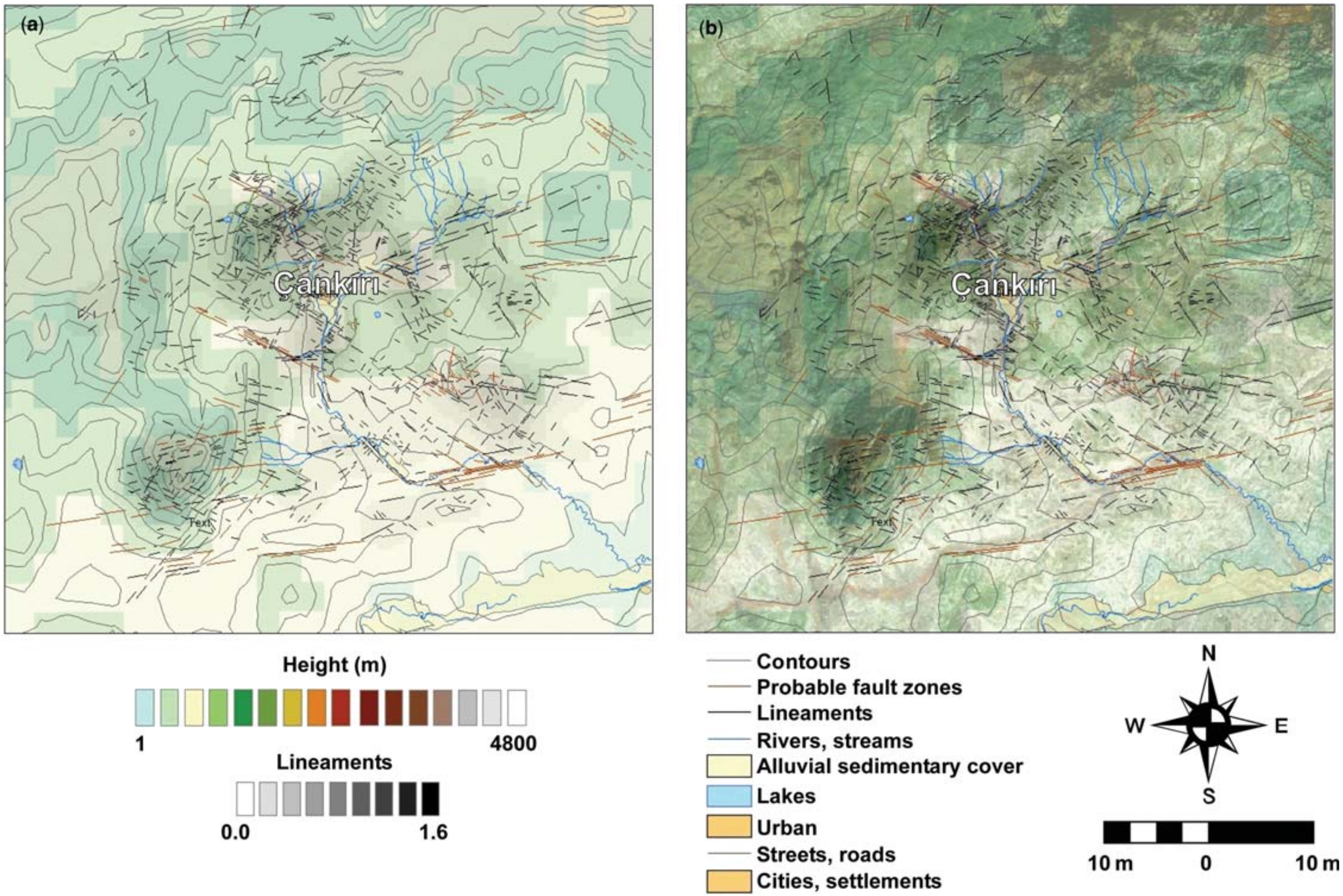

Fig. 13. (**a**) Merged topographic information and structural evaluations based on the LANDSAT ETM image. (**b**) Overlay of LANDSAT ETM, topographic and structural evaluation data.

detail for the purpose of application and maintains a sufficiently large scene size to give the 'overall picture'. The corresponding panchromatic band 8 (15 m) co-registered to the multi-spectral data was used to add crispness and detail to the multi-spectral data. The thermal band has 60 m resolution. The LANDSAT track is 183 km wide.

To enhance the LANDSAT ETM data digital image processing was carried out. Various image sharpening tools (ENVI Software/CREASO) were tested to find the best-suited combinations. The bands 5, 4, 3 (RGB) and 6, 5, 3 (RGB) and 8 were selected to transform to an HSV high-resolution (15 m) image product as shown in Figures 12 and 13. The various datasets (LANDSAT ETM data, and topographic, geological and geophysical data from the study area) were integrated into a GIS using the software ArcView GIS 3.2 with the extensions Spatial Analyst and 3D-Analyst and ArcGIS 8.2 of ESRI to obtain a better understanding of processes influencing the damage intensity of stronger earthquakes.

Lineament analysis

Based on the LANDSAT ETM data for the Orta–Çankırı region, lineament analysis has been carried out. Many of the known faults and fracture zones are traced as linear features and linear arrangements of pixels, especially on amplifications of the satellite images up to a scale of 1:50 000. Linear features are clearly detectable because of the linear arrangements of pixels with the same tone, and/or of linear topographic features such as scarps or drainage pattern. Special attention is focused on areas with distinct expressed lineaments, as well as on those with intersecting lineaments or unconsolidated sedimentary covers. The available data then were merged in a GIS to demonstrate the topographic situation together with tectonic information. The maps show clearly morphological depressions and areas with higher densities of lineaments where stronger ground shaking can be expected. Liquefaction can occur within fluvial sediments (see Fig. 13 for details).

Implications

The rupture process of the 6 June 2000 Orta–Çankırı earthquake (Mw = 6.0) is deduced from the joint inversion of the teleseismic P and SH body waveforms, and separately from InSAR data. We have been able to discriminate between the two possible nodal planes of the fault mechanism parameters. The fault length and rake are also well determined, showing that the earthquake was caused by a mixture of left-lateral strike-slip and normal slip on a north–south-striking fault plane that dips to the east. The fault rake is found to be $-29 \pm 5°$, indicating that the earthquake had a larger component of left-lateral slip than was previously reported by Harvard-CMT and USGS solutions. The magnitude of slip distribution and the depth range of the faulting is well constrained, and the geodetic moment is found to be within the acceptable range of the seismic moment obtained from the teleseismic body-wave inversion results.

The fault plane responsible for the Orta–Çankırı earthquake is at a high angle to that of the North Anatolian Fault, and because of large component of left-lateral slip confirmed by the joint inversion of the teleseismic P and SH body waveforms and InSAR solution, the earthquake slip vector is also oriented at a high angle with respect to slip on the North Anatolian Fault (Fig. 14). However, the horizontal projections of the P- and T-axes of the focal mechanism for the Orta–Çankırı earthquake are similar to those of focal mechanisms summarized in Table 1, suggesting that the same stress regime could be responsible for the earthquakes concerned. One possible interpretation is that right-lateral shear stresses form a shear zone at depth that causes a rotational torque to be applied. This would manifest itself seismically in left-lateral slip on roughly north–south-striking fault planes. In this model, the misalignment between the earthquake slip vectors would be caused by rotation (Fig. 15). Iio *et al.* (2002) also suggested that the observed aftershocks of the 17 August 1999 Gölcük–İzmit earthquake indicate afterslips, which could concentrate larger stress on the source region. Thus, this stress concentration may have triggered the 12 November 1999 Düzce earthquake in conjunction with the stress change caused by the main shock of the Gölcük–İzmit earthquake (e.g. Parsons *et al.* 2000). Similarly uncharacteristic seismic activity

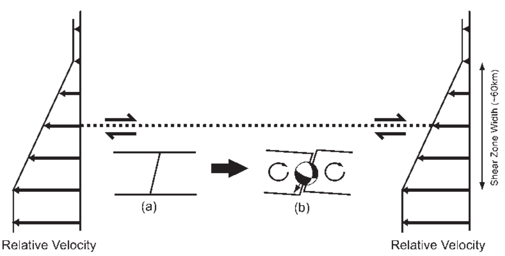

Fig. 14. Schematic diagram (map view) illustrating a possible cause of the Orta–Çankırı earthquake. The velocity arrows indicate the deformation at depth in a 60 km wide shear zone with a strike-slip fault at the centre. The shear zone causes rotational torque to be applied to the upper layer, which could result in an earthquake with the mechanism and slip vector as indicated. (**a**) is the starting condition, and (**b**) is the situation after one earthquake cycle.

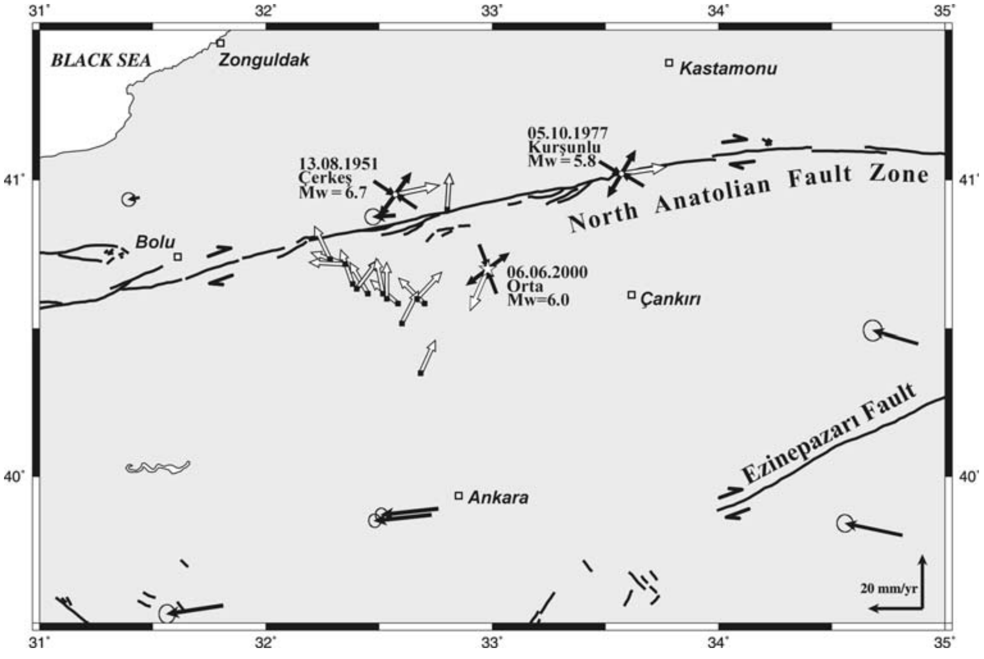

Fig. 15. Summary map showing the horizontal projections of the P- and T-axes and the slip vectors of the Orta–Çankırı earthquake inferred in the present study, and those of nearby earthquakes already reported, shown by bold filled arrows and large open arrows, respectively (see Table 1). Locations of the mapped strands of the North Anatolian Fault (Şaroğlu *et al.* 1992) are shown by bold continuous lines. The small open arrows are palaeomagnetic declinations reported by Platzman *et al.* (1994), obtained from volcanic rocks dated to a Miocene age (7.5–22 Ma). Star indicates the instrumental epicentre of the 6 June 2000 Orta–Çankırı earthquake reported by ISC. The bold filled arrows with error ellipses are interseismic velocities relative to Eurasia measured by GPS (McClusky *et al.* 2000).

is observed in the vicinity of Orta town orthogonal to the known geometry of the North Anatolian Fault Zone (see Fig. 2). Furthermore, Platzman *et al.* (1994) carried out a palaeomagnetic survey on a transect across the North Anatolian Fault close to the Orta–Çankırı earthquake (Fig. 15).

In general, there is no systematic clockwise rotation, but some sites near the Orta–Çankırı earthquake do show clockwise rotations of up to 43°. In addition, it may be concluded that Anatolia has deformed as a fundamentally integral plate subjected to discrete intervals of rotation that would be consistent with the ‘instantaneous’ solution derived from GPS observations. There are conflicting views on the neotectonic crustal deformation in this region. Some researchers have proposed that the region is deformed by differential extrusion and rotation of crustal blocks on a regional scale. Thus, Gürsoy *et al.* (1999) considered that rotations recognized in Eocene units are comparable over a large area of central Anatolia (see Tatar *et al.* 1995) and north of the NAFZ (Sarıbudak 1989; Piper *et al.* 1996, 2001), and they prove to be similar to rotations recognized in younger rocks influenced only by the neo-tectonic regime. Piper *et al.* (2001) considered that central Anatolia shows widespread regional post-Eocene anticlockwise rotations of *c.* 30°. Hence, they argued that rotations are present on either side of the NAFZ, and are therefore older than the establishment of the NAFZ in mid-Pliocene time. Piper *et al.* (2001) further advocated that the character of lithosphere deformation in the region is in conflict with a progressive decline in rotation away from the fault break predicted by the thin viscous sheet model of continental deformation (England & McKenzie 1982). They concluded that the brittle upper crust is detached from the lower crust, undergoes continuum deformation by creep, and the fault blocks are therefore interpreted to be pinned rather than free-floating. It is difficult to compare palaeomagnetic rotations with GPS results, as the former reflect variations on a regional scale with rates of differential rotation many times larger than those of the second. We can then argue that the time period currently investigated by GPS data is too short to yield rotation rates representative of the long-term crustal deformation in Anatolia. In conclusion, these observations suggest that although there is no general clockwise rotation, localized rotations do occur, and these may have been responsible for the Orta–Çankırı earthquake of 6 June 2000.

We thank personnel and station operators at WWSSN, GDSN and IRIS Data Centre for making waveform data available for this study. We are grateful to W. Lee of IASPEI for providing a complimentary copy of IASPEI-Software Library Volume 3: SYN4. We are especially indebted to P. Zwick and R. McCaffrey for helping us on daily matters encountered in use of SYN3, SYN4 and MT5 packages. This research could not have been done without their help. We appreciate Y. Yagi's generous and unselfish offer to let us use his rupture history and slip distribution code. We are grateful to the German Science Foundation (DFG, Bonn), the German Aerospace Centre (DLR, Oberpfaffenhofen) and EUROIMAGE (Rome) for freely providing LANDSAT 7 ETM images from northern central Turkey (Figs 12 and 13), and we thank B. Theilen-Willige for co-operation and discussions. We are also grateful to P. Wessel and W.H.F Smith of Hawaii University–NOAA for providing GMT software (Wessel & Smith 1991, 1995). This research has been partly funded by İstanbul Technical University Research Fund (ITU-BAP), TÜBİTAK, and the Turkish Academy of Sciences (TÜBA), in the framework of the Young Scientist Award Programme (TT/TÜBAGEBİP/2001-2-17). T.J.W. is an NERC (UK) Research Fellow. We also thank B. Parsons, K. Feigl, J. Woodhouse (discussions), ESA (data) and JPL/Caltech (ROI_pac).

References

ADIYAMAN, Ö., CHOROWICZ, J., ARNAUD, O. N., GÜNDOĞDU, M. N. & GOURGAUD, A. 2001. Late Cenozoic tectonics and volcanism along the North Anatolian Fault: new structural and geochemical data. *Tectonophysics*, **338**, 135–165.

AKYÜREK, B., BILGINER, E., ÇATAL, E., DAGER, Z., SOYSAL, Y. & SUNU, O. 1980. *The Geology of Eldivan–Sabanozu (Çankırr) and Hasayaz–Çandır (Kalecik–Ankara) and surrounding regions*. MTA Report 6741 [in Turkish].

ALSDORF, D., BARAZANGI, M., LITAK, R., SEBER, D., SAWAF, T. & AL-SAAD, D. 1995. The intraplate Euphrates fault system–Palmyrides mountain belt junction and relationship to Arabian plate boundary. *Annali di Geofisica*, **38**, 385–397.

AMBRASEYS, N. N. 1970. Some characteristic features of the Anatolian fault zone. *Tectonophysics*, **9**, 143–165.

AMBRASEYS, N. N. & JACKSON, J. A. 1998. Faulting associated with historical and recent earthquakes in the Eastern Mediterranean region. *Geophysical Journal International*, **133**, 390–406.

BOZKURT, E. 2001. Neotectonics of Turkey—a synthesis. *Geodinamica Acta*, **14**, 3–30.

BOZKURT, E. & KOÇYIĞIT, A. 1996. The Kazova basin: an active negative flower structure on the Almus Fault Zone, a splay fault system of the North Anatolian Fault Zone, Turkey. *Tectonophysics*, **265**, 239–254.

BÜRGMANN, R., ROSEN, P. & FIELDING, E. 2000. Synthetic aperture radar interferometry to measure Earth's surface topography and its deformation. *Annual Review of Earth and Planetary Sciences*, **28**, 169–209.

CHANNEL, J. E. T., TÜYSÜZ, O., BEKTAŞ, O. & ŞENGÖR, A. M. C. 1996. Jurassic–Cretaceous paleomagnetism and paleogeography of the Pontides (Turkey). *Tectonics*, **15**, 201–212.

CHOROWICZ, J., DHONT, D. & GÜNDOĞDU, N. 1999. Neotectonics in the eastern North Anatolian fault region (Turkey) advocates crustal extension: mapping from SAR ERS imagery and Digital Elevation Model. *Journal of Structural Geology*, **21**, 511–532.

DEMIRBAĞ, E., RANGIN, C., LE PICHON, X. & ŞENGÖR, A. M. C. 2003. Investigation of the tectonics of the Main Marmara Fault by means of deep-towed seismic data. *Tectonophysics*, **361**, 1–69.

EMRE, Ö., DUMAN, T. Y., DOGAN, A. & ÖZALP, S. 2000. *Evaluation Report of 6 June 2000 Orta (Çankırı-Turkey) Earthquake*. MTA Geology Department, Ankara [in Turkish].

ENGLAND, P. & MCKENZIE, D. P. 1982. A thin viscous sheet model for continental deformation. *Geophysical Journal of the Royal Astronomical Society*, **70**, 295–321.

ERDOĞAN, B., AKAY, E. & UĞUR, M. S. 1996. Geology of the Yozgat region and evolution of the collisional Çankırı basin. *International Geology Review*, **38**, 788–806.

FEIGL, K. L., SERGENT, A. & JACQ, D. 1995. Estimation of an earthquake focal mechanism from a satellite radar interferogram; application to the December 4, 1992 Landers aftershock. *Geophysical Research Letters*, **22**, 1037–1040.

FREDRICH, J., MCCAFFREY, R. & DENHAM, D. 1988. Source parameters of seven large Australian earthquakes determined by body waveforms inversion. *Geophysical Journal*, **95**, 1–13.

FUTTERMAN, W. I. 1962. Dispersive body waves. *Journal of Geophysical Research*, **67**, 5279–5291.

GÖKTEN, E., ÖZAKSOY, V. & KARAKUŞ, K. 1996. Tertiary volcanic and tectonic evolution of the Ayaş–Güdül–Çeltikçi region, Turkey. *International Geology Review*, **38**, 926–934.

GOLDSTEIN, R. M. & WERNER, C. L. 1998. Radar interferogram filtering for geophysical applications. *Geophysical Research Letters*, **25**, 4035–4038.

GÖRÜR, N., TÜYSÜZ, O. & ŞENGÖR, A. M. C. 1998. Tectonic evolution of the Central Anatolian basins. *International Geology Review*, **40**, 831–850.

GÜRSOY, H., PIPER, J. D. A. & TATAR, O. 1999. Palaeomagnetic study of the Galatean Volcanic Province, north–central Turkey: Neogene deformation at the northern border of the Anatolian Block. *Geological Journal*, **34**, 7–23.

HANSSEN, R. F. 2001. *Radar Interferometry: Data Interpretation and Error Analysis*. Kluwer, Dordrecht.

HARTZELL, S. H. & HEATON, T. H. 1983. Inversion of strong ground motion and teleseismic waveform data for fault rupture history of the 1979 Imperial Valley, California, earthquake. *Bulletin of the Seismological Society of America*, **73**, 1553–1583.

IDE, S. & TAKEO, M. 1997. Determination of constitutive relations of fault slip based on seismic wave analysis. *Journal of Geophysical Research*, **102**, 27379–27391.

IMANASHI, K., TAKEO, M., ITO, H. *ET AL.* 2004. Source parameters and rupture velocities of microearthquakes in western Nagano, Japan, determined using stopping phases. *Bulletin of the Seismological Society of America*, **94**, 1762–1780, doi:10.1785/012003085.

IIO, Y., HORIUCHI, S., BARIS, S. *ET AL.* 2002. Aftershock distribution in the eastern part of the aftershock region of the 1999 Izmit, Turkey, earthquake. *Bulletin of the Seismological Society of America*, **92**, 411–417.

JACKSON, J. 1994. Active tectonics of the Aegean region. *Annual Review of Earth and Planetary Sciences*, **22**, 239–271.

JEFFREYS, S. & BULLEN, K. 1940. *Seismological Tables*. British Association for the Advancement of Science, Gray–Milne Trust, London.

JÓNSSON, S., ZEBKER, H., SEGALL, P. & AMELUNG, F. 2002. Fault slip distribution of the 1999 Mw 7.1 Hector Mine earthquake, California, estimated from satellite radar and GPS measurements. *Bulletin of the Seismological Society of America*, **92**, 1377–1389.

KAYMAKÇI, N. 2000. *Tectono-stratigraphical evolution of the Çankırı Basin (Central Anatolia)*. PhD thesis, Universiteit Utrecht.

KAYMAKÇI, N., WHITE, S. H., VANDIJK, P. M. *ET AL.* 2000. Palaeostress inversion in a multiphase deformed area: kinematic and structural evolution of the Çankırı Basin (central Turkey), Part 1—northern area. *In*: BOZKURT, E., WINCHESTER, J. A. & PIPER, J. D. A. (eds) *Tectonics and Magmatism in Turkey and the Surrounding Area.* Geological Society, London, Special Publications, **173**, 295–323.

KAYMAKÇI, N., WHITE, S. H. & VANDIJK, P. M. 2003. Kinematic and structural development of the Çankırı Basin (Central Anatolia, Turkey): a palaeostress inversion study. *Tectonophysics*, **364**, 85–113.

KENNETT, B. L. N. & ENGDAHL, E. R. 1991. Traveltimes for global earthquake location and phase identification. *Geophysical Journal International*, **105**, 429–465.

KIKUCHI, M. & KANAMORI, H. 1991. Inversion of complex body waves—III. *Bulletin of the Seismological Society of America*, **81**, 2335–2350.

KOÇYIĞIT, A. 1991*a*. An example of an accretionary forearc basin from northern central Anatolia and its implications for the history of subduction of Neo-Tethys in Turkey. *Geological Society of America Bulletin*, **103**, 22–36.

KOÇYIĞIT, A. 1991*b*. Changing stress orientation in progressive intracontinental deformation as indicated by the neotectonics of the Ankara region (NW Central Anatolia). *Turkish Association of Petroleum Geologists Bulletin*, **3**, 43–55.

KOÇYIĞIT, A. 1992. Southward-vergent imbricate thrust zone in Yuvaköy: a record of the latest compressional event related to the collisional tectonic regime in Ankara–Erzincan Suture Zone. *Turkish Association of Petroleum Geologists Bulletin*, **4**, 111–118.

KOÇYIĞIT, A., TÜRKMENOĞLU, A., BEYHAN, A., KAYMAKÇI, N. & AKYOL, E. 1995. Post-collisional tectonics of Eskisehir–Ankara–Çankırı segment of Izmir–Ankara–Erzincan suture zone: Ankara Orogenic Phase. *Turkish Association of Petroleum Geologists Bulletin*, **6**, 69–86.

KOÇYIĞIT, A., ROJAY, B., CIHAN, M. & ÖZACAR, A. 2001. The June 6, 2000, Orta (Çankırı, Turkey) earthquake: sourced from a new antithetic sinistral strike-slip structure of the North Anatolian Fault System, the Dodurga Fault Zone. *Turkish Journal of Earth Sciences*, **10**, 69–82.

KURT, H., DEMIRBAĞ, E. & KUŞÇU, I. 1999. Investigation of the submarine active tectonism in the Gulf of Gökova, Southwest Anatolia–Southeast Aegean Sea, by multi-channel seismic reflection data. *Tectonophysics*, **305**, 477–496.

KURT, H., DEMIRBAĞ, E. & KUŞÇU, İ. 2000. Active submarine tectonism and formation of the Gulf of Saros; Northeast Aegean Sea; inferred from multi-channel seismic reflection data. *Marine Geology*, **165**, 13–26.

LAY, T. & WALLACE, T. C. 1995. *Modern Global Seismology.* Academic Press, San Diego, CA.

LEE, W. H. K. (ed.) 1991. *IASPEI Software Library Volume 3, Digital Seismogram Analysis and Waveform Inversion*. IASPEI Working Group on Personal Computers, Menlo Park, CA.

LE PICHON, X., LYBERIS, N. & ALVAREZ, F. 1984. Subsidence history of the North Aegean trough. *In*: DIXON, J. E. & ROBERTSON, A. H. F. (eds) *The Geological Evolution of the Eastern Mediterranean*. Geological Society, London, Special Publications, **17**, 27–741.

LE PICHON, X., ŞENGÖR, A. M. C., DEMIRBAĞ, E. *ET AL.* 2001. The active Main Marmara Fault. *Earth and Planetary Science Letters*, **192**, 595–616.

MAKRIS, J. & STOBBE, C. 1984. Physical properties and state of the crust and upper mantle of the Eastern Mediterranean Sea deduced from geophysical data. *Marine Geology*, **55**, 347–363.

MASSONET, D. & FEIGL, K. L. 1998. Radar interferometry and its application to changes in the Earth's surface. *Review of Geophysics*, **36**, 441–500.

MASSONET, D., ROSSI, M., CARMONA, C., ADRAGNA, F., PELTZER, G., FEIGL, K. & RABAUTE, T. 1993. The displacement field of the Landers earthquake mapped by radar interferometry. *Nature*, **364**, 138–142.

MCCAFFREY, R. 1988. Active tectonics of the Eastern Sunda and Banda Arcs. *Journal of Geophysical Research*, **93**, 15163–15182.

MCCAFFREY, R. & ABERS, G. 1988. *SYN3: a program for inversion of teleseismic body wave forms on micro-computers*. US Air Force Geophysics Laboratory Technical Report, **AFGL-TR-88-0099**.

MCCAFFREY, R. & NÁBĚLEK, J. 1987. Earthquakes, gravity, and the origin of the Bali Basin: an example of a nascent continental fold-and-thrust belt. *Journal of Geophysical Research*, **92**, 441–460.

MCCLUSKY, S., BALASSANIAN, S., BARKA, A. *ET AL.* 2000. Global positioning system constraints on plate kinematics and dynamics in the eastern Mediterranean and Caucasus. *Journal of Geophysical Research*, **105**, 5695–5719.

MCKENZIE, D. 1969. The relation between fault plane solutions for earthquakes and the directions of the principal stresses. *Bulletin of the Seismological Society of America*, **59**, 591–601.

McKenzie, D. 1970. Plate tectonics of the Mediterranean region. *Nature*, **226**, 239–243.

McKenzie, D. 1972. Active tectonics of the Mediterranean region. *Geophysical Journal of the Royal Astronomical Society*, **30**, 109–185.

Mercier, J. L., Sorel, D., Vergely, P. & Simeakis, K. 1989. Extensional tectonic regimes in the Aegean basins during the Cenozoic. *Basin Research*, **2**, 49–71.

Molnar, P. & Lyon-Caen, H. 1989. Fault plane solutions of earthquakes and active tectonics of the Tibetan Plateau and its margins. *Geophysical Journal International*, **99**, 123–153.

Nábělek, J. L. 1984. *Determination of earthquake source parameters from inversion of body waves*. PhD thesis, Massachusetts Institute of Technology, Cambridge, MA.

Nelson, M. R., McCaffrey, R. & Molnar, P. 1987. Source parameters for 11 earthquakes in the Tien Shan, central Asia, determined by P and SH waveform inversion. *Journal of Geophysical Research*, **92**, 12629–12648.

Nemec, W. & Kazanci, N. 1999. Quaternary colluvium in west–central Anatolia: sedimentary facies and paleoclimatic significance. *Sedimentology*, **46**, 139–170.

Nowroozi, A. A. 1972. Focal mechanism of earthquakes in Persia, Turkey, west Pakistan and Afghanistan and plate tectonics of the Middle East. *Bulletin of the Seismological Society of America*, **62**, 823–850.

Okada, Y. 1985. Surface deformation due to shear and tensile faults in a half-space. *Bulletin of the Seismological Society of America*, **75**, 1135–1154.

Okay, A. I. & Tüysüz, O. 1999. Tethyan sutures of northern Turkey. *In*: Durand, B., Jolivet, L., Horvath, F. & Serrane, M. (eds) *The Mediterranean Basins: Tertiary Extension within the Alpine Orogen*. Geological Society, London, Special Publications, **156**, 475–515.

Özay, İ. 1996. *Source parameters of 1977 October 5 Kurşunlu (NW Turkey) earthquake*. BSc Thesis, İstanbul Technical University.

Papazachos, B. C., Papadimitriou, E. E., Kiratzi, A. A., Papazachos, C. B. & Louvari, E. K. 1998. Fault plane solutions in the Aegean Sea and the surrounding area and their implication. *Bolletino di Geofisica Teorica ed Applicata*, **39**, 199–218.

Parsons, T., Toda, S., Stein, R., Barka, A. & Dieterich, J. 2000. Heightened odds of large earthquakes near Istanbul: an interaction-based probability calculation. *Science*, **288**, 661–665.

Piper, J. D. A., Moore, J., Tatar, O., Gürsoy, H. & Park, G. 1996. Palaeomagnetic study of crustal deformation across an intracontinental transform: the North Anatolian Fault Zone in Northern Turkey. *In*: Morris, A. & Tarling, D. H. (eds) *Palaeomagnetism of the Mediterranean Regions.* Geological Society, London, Special Publications, **105**, 191–203.

Piper, J. D. A., Gürsoy, H. & Tatar, O. 2001. Palaeomagnetic analysis of neotectonic crustal deformation in Turkey. *In*: Taymaz, T. (ed.) *Symposia on Seismotectonics of the North-Western Anatolia–Aegean and Recent Turkish Earthquakes, Extended Abstracts*. Istanbul Technical University, Istanbul, 4–13.

Platzman, E. S., Platt, J. P., Tapirdamaz, C., Sanver, M. & Rundle, C. C. 1994. Why are there no clockwise rotaions along the North Anatolian Fault Zone? *Journal of Geophysical Research*, **99**, 21705–21715.

Polat, A. 1988. Evidence for paleo- to neotectonic transition period in the Büyük Polat-Yarımsöğüt region and the origin of the Kırıkkale–Erbaa Fault Zone. *Turkish Association of Petroleum Geologists Bulletin*, 127–140.

Price, S. P. & Scott, B. 1994. Fault-block rotations at the edge of a zone of continental extension; southwest Turkey. *Journal of Structural Geology*, **16**, 381–392.

Richens, W. D., Pechmann, J. C., Smith, R. B., Langer, C. J., Goter, S. K., Zollweg, J. E. & King, J. J. 1987. The Borah Peak, Idaho, earthquake and its aftershocks. *Bulletin of the Seismological Society of America*, **77**, 694.

Saribudak, M. 1989. A paleomagnetic approach to the origin of the Black Sea. *Geophysical Journal International*, **99**, 247–251.

Şaroğlu, F., Emre, Ö. & Kuşçu, İ. 1992. *Active Fault Map of Turkey, 2 sheets*. Maden ve Tetkik Arama Enstitüsü, Ankara.

Şen, Ş., Seyitoğlu, G., Karadenizli, L., Kazanci, N., Varol, B. & Araz, H. 1998. Mammalian biochronology of Neogene deposits and its correlation with the lithostratigraphy in the Çankırı–Çorum basin, central Anatolia, Turkey. *Eclogae Geologicae Helvetiae*, **91**, 307–320.

Şengör, A. M. C. 1979. The north Anatolian transform fault: its age, offset and tectonic significance. *Journal of the Geological Society, London*, **136**, 269–282.

Şengör, A. M. C. & Yilmaz, Y. 1981. Tethyan evolution of Turkey: a plate tectonic approach. *Tectonophysics*, **75**, 181–241.

Şengör, A. M. C., Görür, N. & Şaroğlu, F. 1985. Strike-slip faulting and related basin formation in zones of tectonic escape: Turkey as a case study. *In*: Biddle, K. T. & Christie-Blick, N. (eds) *Strike-Slip Deformation, Basin Formation, and Sedimentation*. Society of Economic Paleontologists and Mineralogists, Special Publications, **37**, 227–264.

Seyitoğlu, G., Kazanci, N., Fodor, L., Karakuş, K., Araz, H. & Karadenizli, L. 1997. Does continuous compressive tectonic regime exist during late Paleogene to late Neogene in NW central Anatolia, Turkey? *Turkish Journal of Earth Sciences*, **6**, 77–83.

Seyitoğlu, G., Kazanci, N., Karadenizli, L., Şen, S., Varol, B. & Karabiyikoğlu, T. 2000. Normal fault induced rockfall avalanche deposits in the NW of Çankırı basin (central Turkey) and their implications for the post-collisional tectonic evolution of the Neo-Tethyan suture zone. *Terra Nova*, **12**, 245–251.

Seyitoğlu, G., Kazanci, N., Karadenizli, L., Şen, S. & Varol, B. 2001. A Neotectonic pinched crustal wedge in the west of Cankırı basin accommodating the intemal deformation of Anatolian Plate. *Fourth International Turkish Geology Symposium, Abstracts*. Çukurova University, Turkey, p. 103.

SMITH, W. H. F. & SANDWELL, D. T. 1997. Global seafloor topography from satellite altimetry and ship depth soundings. *Science*, **277**, 1957–1962.

STEIN, R. S., BARKA, A. A. & DIETERICH, J. D. 1997. Progressive failure on the North Anatolian fault since 1939 by earthquake stress triggering. *Geophysical Journal International*, **128**, 594–604.

TAN, O. 1996. *Source parameters of 1968 September 3 Bartın (NW Turkey) earthquake.* BSc thesis, İstanbul Technical University.

TATAR, O., PIPER, J. D. A., PARK, R. G. & GÜRSOY, H. 1995. Palaeomagnetic study of block rotations in the Niksar overlap region of the North Anatolian Fault Zone, central Turkey. *Tectonophysics*, **244**, 251–256.

TAYMAZ, T. 1990. *Earthquake source parameters in the Eastern Mediterranean region.* PhD thesis, University of Cambridge.

TAYMAZ, T. 1993. The source parameters of Çubukdağ (Western Turkey) earthquake of 11 October 1986. *Geophysical Journal International*, **113**, 260–267.

TAYMAZ, T. & PRICE, S. 1992. The 1971 May 12 Burdur earthquake sequence, SW Turkey: a synthesis of seismological and geological observations. *Geophysical Journal International*, **108**, 589–603.

TAYMAZ, T. & TAN, O. 2001. Source parameters of June 6, 2000 Orta–Çankırı (Mw = 6.0) and December 15, 2000 Sultandağ–Akşehir (Mw = 6.0) earthquakes obtained from inversion of teleseismic P- and SH waveforms. *In*: TAYMAZ, T. (ed.) *Symposia on Seismotectonics of the North-Western Anatolia–Aegean and Recent Turkish Earthquakes, Extended Abstracts.* Istanbul Technical University, Istanbul, 96–107.

TAYMAZ, T., JACKSON, J. A. & WESTAWAY, R. 1990. Earthquake mechanisms in the Hellenic Trench near Crete. *Geophysical Journal International*, **102**, 695–731.

TAYMAZ, T., JACKSON, J. A. & MCKENZIE, D. 1991*a*. Active tectonics of the North and Central Aegean Sea. *Geophysical Journal International*, **106**, 433–490.

TAYMAZ, T., EYIDOĞAN, H. & JACKSON, J. 1991*b*. Source parameters of large earthquakes in the East Anatolian Fault Zone (Turkey). *Geophysical Journal International*, **106**, 537–550.

TAYMAZ, T., WRIGHT, T., TAN, O., FIELDING, E. & SEYITOĞLU, G. 2002*a*. Source characteristics of Mw = 6.0 June 6, Orta–Çankırı (Central Turkey) earthquake: a synthesis of seismological, geological and geodetic (InSAR) observations, and internal deformation of Anatolian plate. *In*: *1st International Symposium of Istanbul Technical University the Faculty of Mines on Earth Sciences and Engineering, Abstracts Book*. Istanbul Technical University, Istanbul, 63.

TAYMAZ, T., TAN, O., ÖZALAYBEY, S. & KARABULUT, H. 2002*b*. Source characteristics of February 3, 2002 Çay–Sultandağı earthquake (Mw = 6.5) sequence in SW Turkey: a synthesis of seismological observations of body-waveforms, strong motions, and aftershock seismicity survey data. *In*: *1st International Symposium of Istanbul Technical University the Faculty of Mines on Earth Sciences and Engineering, Abstracts Book.* Istanbul Technical University, Istanbul, 60, Turkey.

TAYMAZ, T., WESTAWAY, R. & REILINGER, R. (eds) 2004. Active faulting and crustal deformation in the Eastern Mediterranean region. *Tectonophysics* (special issue), **391**,

TÜRKECAN, A., HEPŞEN, N., PAPAK, İ. *ET AL.* 1991. *Geology and petrology of volcanic rocks of Seben–Gerede (Bolu)–Güdül–Beypazarı (Ankara and Çerkeş–Orta–Kurşunlu, Çankırı and surrounding regions.* MTA Report 9193 [in Turkish].

WELLS, D. L. & COPPERSMITH, K. 1994. New empirical relationships among magnitude, rupture length, rupture width, rupture area, and surface displacement. *Bulletin of the Seismological Society of America*, **84**, 974–002.

WESSEL, P. & SMITH, W. H. F., 1991. Free software helps map and display data. *EOS Transactions, American Geophysical Union*, **72**, 441, 445–446.

WESSEL, P. & SMITH, W. H. F. 1995. New version of the generic mapping tools released. *EOS Transactions, American Geophysical Union*, **76**, 329.

WILSON, M., TANKUT, A. & GÜLEÇ, N. 1997. Tertiary volcanism of the Galatia province, north-west central Anatolia, Turkey. *Lithos*, **42**, 105–121.

WRIGHT, T. J. 2002. Remote monitoring of the earthquake cycle using satellite radar interferometry. *Philosophical Transactions of the Royal Society of London, Series A*, **360**, 2873–2888.

WRIGHT, T. J., PARSONS, B., JACKSON, J., HAYNES, M., FIELDING, E., ENGLAND, P. & CLARKE, P. 1999. Source parameters of the 1 October 1995 Dinar (Turkey) earthquake from SAR interferometry and seismic body-wave modelling. *Earth and Planetary Science Letters*, **172**, 23–37.

WRIGHT, T. J., PARSONS, B. & FIELDING, E. 2001*a*. The 1999 Turkish earthquakes: source parameters from InSAR and observations of triggered slip. *In*: TAYMAZ, T. (ed.) *Symposia on Seismotectonics of the North-Western Anatolia-Aegean and Recent Turkish Earthquakes*, *Extended Abstracts*. Istanbul Technical University, Istanbul, 54–71.

WRIGHT, T. J., FIELDING, E. J. & PARSONS, B. 2001*b*. Triggered slip: observations of the 17 August 1999 İzmit (Turkey) earthquake using radar interferometry. *Geophysical Research Letters*, **28**, 1079–1082.

YAGI, Y. 2000. Source process of large earthquakes (aseismic and coseismic slip). PhD thesis, University of Tokyo.

YAGI, Y. & KIKUCHI, M. 2000. Source rupture process of the Kocaeli, Turkey, earthquake of August 17, 1999, obtained by joint inversion of near-field data and teleseismic data. *Geophysical Research Letters*, **27**, 1969–1972.

YOSHIDA, S., KOKETSU, K., SHIBAZAKI, B., SAGIYA, T., KATO, T. & YOSHIDA, Y. 1996. Joint inversion of near- and far-field waveforms and geodetic data for rupture processes of the 1995 Kobe earthquakes. *Journal of Physics of the Earth*, **44**, 437–457.

ZEBKER, H., ROSEN, P., GOLDSTEIN, R., GABRIEL, R. & WERNER, C. 1994. On the derivation of coseismic displacement fields using differential radar interferometry: the Landers earthquake. *Journal of Geophysical Research*, **99**, 19617–19634.